

Higher-order corrections to jet cross sections in e^+e^- annihilation

W. T. Giele

Fermi National Accelerator Laboratory, P.O. Box 500, Batavia, Illinois

E. W. N. Glover

Physics Department, University of Durham, Durham DH1 3LE, England

(Received 23 March 1992)

A general method to calculate next-to-leading-order multijet cross sections is presented. The emphasis is on how to isolate the soft and collinear divergences in multiparton matrix elements at all orders in the number of colors. As an example, the method is used to isolate the divergences in $e^+e^- \rightarrow q\bar{q} + n$ gluons and $e^+e^- \rightarrow q\bar{q}q\bar{q} + n$ gluons, where, for simplicity we keep only the terms at leading order in the number of colors. The usual algebraic complexity of calculating next-to-leading-order corrections in QCD is avoided, especially the d -dimensional squaring of the real matrix elements and the hard phase-space integrals. Some remarks about the structure of the virtual contributions are made. As a first application, and to examine the feasibility of the approach, explicit Monte Carlo programs are constructed which contain the complete next-to-leading-order corrections to $e^+e^- \rightarrow 2$ jets and $e^+e^- \rightarrow 3$ jets. It is demonstrated that the method works and can be readily applied to a variety of processes.

PACS number(s): 13.87.Ce, 12.38.Bx, 13.65.+i

I. INTRODUCTION

By the use of a suitable experimental jet definition, it is possible to classify experimental data in terms of the number of observed jets. For example, the processes

$$p\bar{p} \rightarrow n_1 \text{ jets}, \quad (1.1)$$

$$p\bar{p} \rightarrow W/Z + n_2 \text{ jets}, \quad (1.2)$$

and,

$$e^+e^- \rightarrow n_3 \text{ jets}, \quad (1.3)$$

have been observed for $n_1 \leq 6$ [1], $n_2 \leq 4$ [2] and $n_3 \leq 5$ [3]. It is then a theoretical challenge to compute exclusive jet cross sections with sufficient precision to compare with the data. Moreover these multijet final states often are a background to new physics. Therefore a good understanding of multijet final states is of the utmost importance.

One immediate problem is that perturbative QCD predicts parton cross sections, while experimentally one observes only hadrons. As yet the hadronization process is only known phenomenologically and, therefore, one cannot directly relate theory and experiment. Although there is an approximate correspondence between the underlying parton configuration and the hadronic structure of the event, one must always bear hadronization effects in mind when computing multiple-jet cross sections at the parton level.

The lowest-order matrix elements for (1.1)–(1.3) have been computed for $n_1 \leq 5$ [4–10], $n_2 \leq 4$ [11–14] and $n_3 \leq 5$ [15, 16, 12, 13, 17] by making use of helicity amplitudes [18], color decompositions [7, 8, 19] and recursion relations [20, 10] to control the rapid increase in the number of contributing Feynman diagrams as the number of

partons involved grows. The cross section is obtained by Monte Carlo integration over all the final-state partons, and, at this order, the individual partons are identified as jets. The experimental acceptances and jet algorithms are then directly applied and, since the jet four-momenta are known, one can study any distribution such as the average transverse jet momentum or the two-jet invariant mass. Comparisons with the data have proved reasonable, bearing in mind the fact that one is comparing a parton level calculation with hadronic data. In general, the lowest-order matrix elements predict shapes of distributions reasonably well. However, because of the uncertainties related to the scale choice μ at which we evaluate the strong coupling constant $\alpha_s(\mu^2)$, the overall normalization is uncertain.

In principle, the normalization is better predicted once higher-order QCD corrections are included since the scale dependence tends to cancel amongst the contributions at different order in the coupling constant. On the other hand, as higher-order corrections are included, more and more partons are admitted into the final state. In contrast with the lowest-order interpretation, the partons may be soft and/or collinear and cannot be directly identified as jets. The question then arises of how to define a jet cross section at higher order. Clearly this should be done in such a way that the parton shower is perturbatively reconstructed and each jet should contain more and more partons. By doing this, the average energy flow around the jet will be correctly modeled and the jet cross sections will be sensitive to the jet-defining algorithm.

Since the jet is made up of partons, it is also necessary to define a parton in higher orders. A natural definition is to introduce a parton resolution criteria to define when a parton is resolved either as a single hard parton or as a cluster of partons. A practical consequence of this is that divergences associated with the soft and/or collinear

partons can be isolated and analytically canceled against the divergences from the virtual graphs. In dimensional regularization [21, 22], which entails working in $d = 4 - 2\epsilon$ dimensions, these divergences are associated with poles in $1/\epsilon^m$. After the analytic cancellation, the resolved parton matrix elements contain no poles in $1/\epsilon$ and may therefore be evaluated in the 4-dimensional limit. Similarly, the phase space is 4-dimensional but restricted by the parton resolution criteria.

As in lowest order, one can then directly apply Monte Carlo methods to compute the jet cross section. For example, at next-to-leading order, the n -jet cross section receives contributions from the n -parton and $(n + 1)$ -parton final states. In each case, the experimental jet algorithms can be applied to the parton momenta to obtain jet momenta, which may or may not be the result of clustering partons together. The next-to-leading-order jet cross section is therefore fully differential.

It is important to note that the parton resolution criteria is totally unrelated to any experimental jet definition. Furthermore, although the n -parton and $(n + 1)$ -parton cross sections depend logarithmically on the resolution criteria, the physical jet cross section does not.

In Sec. II we will define the exclusive jet cross sections to all orders in perturbation theory and discuss the physical picture behind the introduction of a parton resolution criteria. We use this parton resolution criteria to isolate the divergences which occur when one of the partons is either soft or collinear with one of the other partons [23] and is therefore unresolved (Sec. III). As we will show, these divergences have a universal structure and multiply the lowest-order matrix elements in a nontrivial way. Although our scheme is applicable to partons in the initial state, for now we will focus on final-state partons alone. In particular, we will isolate the singularities at leading order in the number of colors for

$$e^+e^- \rightarrow q\bar{q} + ng, \quad (1.4)$$

and

$$e^+e^- \rightarrow q\bar{q}q\bar{q} + (n - 2)g, \quad (1.5)$$

when one of the partons is unresolved. In Sec. IV, we will show how to extract the most singular ($1/\epsilon^2$) poles from the virtual one-loop graphs contributing to (1.4) and (1.5). These poles arise when a virtual gluon within the loop becomes soft, and ultimately cancel against the real soft gluon contributions of Sec. II. As an explicit example, we will apply our results to $e^+e^- \rightarrow 2$ jets at $O(\alpha_s)$ and $e^+e^- \rightarrow 3$ jets at $O(\alpha_s^2)$ in Sec. V, where we show some numerical results from the next-to-leading-order Monte Carlo calculation. In particular, we will demonstrate that distributions of jet observables are independent of the parton resolution criteria. Finally, we summarize our results and indicate possible extensions in Sec. VI. Helicity amplitudes for the relevant matrix elements are collected in the Appendix.

II. DEFINING EXCLUSIVE JET CROSS SECTIONS

In order to calculate exclusive jet cross sections it is necessary to define the cross section up to all orders in

perturbation theory. Of course we define only the perturbatively calculable part of the jet which is the parton shower. The subsequent hadronization is not in the realm of perturbative QCD.

In lowest order, it is clear how to define the jet cross section since the whole parton shower is modeled by a single parton and we must therefore identify each outgoing parton as a jet and this implies that we must apply the jet-defining cuts to each individual parton. In other words, there is only one parton in each jet cone which carries all the jet energy and momentum; the jet axis is thus identified with the parton four-momentum. Any sensible experimental jet algorithm should reproduce the lowest-order results in a global way.

A simple example of an exclusive jet cross section, which we will use throughout the paper, is e^+e^- annihilation into three jets, for which the lowest-order contribution is the order- α_s process $e^+e^- \rightarrow q\bar{q}g$. One possible jet definition is a minimum mass cut such that the invariant mass of any jet pair is larger than an experimentally defined minimum s_{cut} :

$$s_{j_1 j_2} = (P_{j_1} + P_{j_2})^2 > s_{\text{cut}}, \quad (2.1)$$

where P_{j_i} is the four-momentum of jet i . This translates down to the parton level by demanding that the three possible invariant masses that can be constructed from the parton momenta are all larger than the minimum invariant mass s_{cut} . This more or less ensures that the subsequent hadronization of these partons will result in three distinct showers which are experimentally identified as jets. This means that the three-jet cross section is given in lowest order by

$$d\sigma_1(e^+e^- \rightarrow 3 \text{ jets}) = \Theta d\sigma_1(e^+e^- \rightarrow q\bar{q}g), \quad (2.2)$$

where Θ contains the experimental jet definition for a three-jet final state,

$$\Theta = \theta(s_{q\bar{q}} - s_{\text{cut}})\theta(s_{qg} - s_{\text{cut}})\theta(s_{\bar{q}g} - s_{\text{cut}}), \quad (2.3)$$

with s_{ij} the invariant mass of partons i and j and $d\sigma_1(e^+e^- \rightarrow q\bar{q}g)$ is the $O(\alpha_s)$ leading-order cross section for $e^+e^- \rightarrow q\bar{q}g$. The step function $\theta(x)$ is 1 for $x \geq 0$ and 0 otherwise.

It is clear that it is necessary and desirable to extend the above scheme to include higher-order corrections. This gives two distinct improvements. The first one stems from the fact that by increasing the order of perturbation theory the dependence on the scale choice μ at which we evaluate $\alpha_s(\mu^2)$ is reduced. The second improvement results from the fact that a jet is a relatively "fat" object in phase space and may contain more than one parton. In fact, by increasing the order in α_s , we begin to reconstruct the parton shower. In other words, instead of modeling the shower by one hard parton we describe the shower by more partons. This will improve the predictive power of the calculation because it becomes more and more sensitive to the details of the jet finding algorithm. Eventually, adding all orders, this scheme describes the full parton shower.

Let us first look at what happens in our example $e^+e^- \rightarrow 3$ jets. We saw that in lowest order all the contributions to the jet cross section come from the parton process $e^+e^- \rightarrow q\bar{q}g$. At next-to-leading order, there

are two contributions. One contribution comes from the real diagrams (i.e., the tree-level four-parton processes, $e^+e^- \rightarrow q\bar{q}gg$ and $e^+e^- \rightarrow q\bar{q}q\bar{q}$ [15, 16]). There are two distinct possibilities in which the four-parton processes will not contribute to the lowest-order four-jet cross section but to the $O(\alpha_s^2)$ correction to the three-jet cross section. First of all, we can have two almost collinear partons within one jet. Depending on the clustering algorithm they will be combined to reconstruct the jet axis and energy. The other possibility is a soft parton outside the jet cones. This will model the energy flow between the jets. Each of these contributions gives a divergent contribution to the three-jet cross section. However, at the same order in α_s , the virtual graphs also provide a divergent contribution which precisely cancels the divergences arising from the soft and collinear regions [16]. Finally, after coupling constant renormalization, a finite three jet cross section is obtained.

The above scheme has clear disadvantages since we must integrate out the collinear partons within a jet according to the clustering algorithm to obtain the contribution to a given three jet configuration. Also the soft radiation has to be integrated out. The resulting $O(\alpha_s^2)$ differential three jet cross section is then given by

$$d\sigma_2(e^+e^- \rightarrow 3 \text{ jets}) = \Theta \left[d\sigma_2^V(e^+e^- \rightarrow 3 \text{ partons}) + \int d\sigma_2(e^+e^- \rightarrow 4 \text{ partons}) \right], \quad (2.4)$$

where, $d\sigma_2^V(e^+e^- \rightarrow 3 \text{ partons})$ is the divergent virtual $O(\alpha_s^2)$ cross section and $d\sigma_2(e^+e^- \rightarrow 4 \text{ partons})$ is the tree level $e^+e^- \rightarrow q\bar{q}gg$ and $e^+e^- \rightarrow q\bar{q}q\bar{q}$ cross section. The integration represents the projection of four-parton phase space onto three-jet phase space. In practice, this is a very difficult and probably impossible calculation because of the severe phase space constraints on projecting the contributions from the four-parton matrix elements onto the three-jet phase space. So one is restricted to integrating out the final state without defining the jets (such as event shapes [16, 24]). Alternatively, we could have chosen jet-defining cuts and clustering algorithms and analytically computed the three-jet cross section [25, 26]. However, often one wants to change the jet algorithm

or try several of them and this would require redoing the calculation. Furthermore, the detector often has some difficult acceptance cuts which can have serious effects on the measurements. It is impossible to include these constraints in the analytic calculation.

At tree level we did not have these problems since the parton momentum was directly identified with the jet momentum. Therefore the jet definition and phase space integration can be performed numerically with the aid of Monte Carlo techniques. We want to do this for the higher-order corrections as well. Therefore we will define higher-order parton cross sections instead of jet cross sections. With these parton cross sections we can then (using the same Monte Carlo techniques as in lowest order) obtain the physically measurable jet cross sections. So, instead of interpreting the lowest order as a jet cross section, we view it as a parton cross section and generalize from that viewpoint. Of course the parton cross section has no physical meaning and only after defining the jets and performing the numerical integration to obtain the jet cross section do we obtain a physically meaningful result.

In order to obtain a parton-level higher-order cross section, we have to define the concept of a parton in higher orders. To do this we will envision an experiment with a parton detector (i.e., a detector which detects individual partons). This will guide us to the right concept of a higher-order (or *dressed*) parton. Any detector has a finite resolution, and our parton detector can resolve two partons as individual partons if and only if the invariant mass of the parton pair is larger than the quantity s_{\min} . If the invariant mass of the pair of partons is smaller than s_{\min} the partons are unresolved and detected as a single parton. No matter how small we choose s_{\min} , if we include all orders there will always be an infinite number of partons within this invariant mass. The quantum corrections will always render the final answer finite. Note that this resembles a jet, the shower is replaced by a single parton to model the behavior of the unresolved parton shower.

To see exactly how this works, let us return to our example of $e^+e^- \rightarrow 3 \text{ jets}$ (2.4). In this case, the four-parton phase space splits up into a part where all four partons are resolved, one where only three are seen and one where only two are observed. Schematically,

$$d\sigma_2(e^+e^- \rightarrow 4 \text{ partons}) = \left[\prod_{ij} [\theta(s_{ij} - s_{\min}) + \theta(s_{\min} - s_{ij})] \right] d\sigma_2(e^+e^- \rightarrow 4 \text{ partons}) \\ = \left[\prod_{ij} \theta(s_{ij} - s_{\min}) + \sum_{kl} \theta(s_{\min} - s_{kl}) \prod_{ij \neq kl} \theta(s_{ij} - s_{\min}) \right. \\ + \sum_{kl, km} \theta(s_{\min} - s_{kl}) \theta(s_{\min} - s_{km}) \prod_{ij \neq kl, km} \theta(s_{ij} - s_{\min}) \\ + \sum_{kl, km, kn} \theta(s_{\min} - s_{kl}) \theta(s_{\min} - s_{km}) \theta(s_{\min} - s_{kn}) \prod_{ij \neq kl, km, kn} \theta(s_{ij} - s_{\min}) \\ \left. + \dots \right] d\sigma_2(e^+e^- \rightarrow 4 \text{ partons}), \quad (2.5)$$

where the sum (product) runs over the different parton pairs. In this equation, the first term represents the contribution to the four-parton cross section when all four partons are resolved, $d\sigma_2^R(e^+e^- \rightarrow 4 \text{ partons})$. The second and third terms represent the divergent contributions when one of the partons is either collinear or soft respectively, $d\sigma_2^C(e^+e^- \rightarrow 3 \text{ partons})$ and $d\sigma_2^S(e^+e^- \rightarrow 3 \text{ partons})$ and only three partons are resolved. Partons i and j are collinear when $s_{ij} < s_{\min}$, while parton k is soft when at least two invariants are unresolved, $s_{kl} < s_{\min}$ and $s_{km} < s_{\min}$. The fourth term also represents configurations when parton k is soft while the three remaining partons are resolved. However, as we will see later, in the soft limit the matrix elements contain double poles in any pair of invariants s_{kl} , s_{km} , and s_{kn} but never in all three simultaneously as follows directly from the matrix

elements. This term therefore generates a contribution of $O(s_{\min})$ and is negligible. The terms not shown are when two partons are unresolved, either two collinear pairs or two soft partons or one soft and one collinear pair, and therefore contribute to the $O(\alpha_s^2)$ two-parton cross section.

Since all we have done is to divide up the phase space in an arbitrary way, the jet cross section cannot depend on s_{\min} . However taking the $s_{\min} \rightarrow 0$ limit simplifies the calculation considerably, since now we can neglect terms which disappear as $s_{\min} \rightarrow 0$. Furthermore we can make use of collinear and soft factorizations of the matrix elements which are only valid in this approximation.

By relabeling the hard partons and integrating out the unresolved partons, the full $O(\alpha_s^2)$ cross section for three resolved partons is given by

$$d\sigma_2^R(e^+e^- \rightarrow 3 \text{ partons}) = \prod_{ij} \theta(s_{ij} - s_{\min}) [d\sigma_2^V(e^+e^- \rightarrow 3 \text{ partons}) + d\sigma_2^C(e^+e^- \rightarrow 3 \text{ partons}) + d\sigma_2^S(e^+e^- \rightarrow 3 \text{ partons})]. \quad (2.6)$$

Because of the Bloch-Nordsieck [27] and Kinoshita-Lee-Nauenberg [28] theorems, the soft and collinear poles cancel against the virtual contributions to yield a finite result after the usual coupling constant renormalization. A somewhat stronger theorem for the cancellation of the mass divergences was given in [29] where the divergences were shown to cancel on a point-by-point basis between the phase space for physical particles and loop momentum space for virtual particles. In fact, as we will show in the next sections, the divergences are all proportional to the lowest-order three-parton cross section and may be explicitly isolated in d dimensions and analytically canceled, so that,

$$d\sigma_2^R(e^+e^- \rightarrow 3 \text{ partons}) = \prod_{ij} \theta(s_{ij} - s_{\min}) [\mathcal{K}(s_{q\bar{q}}, s_{qg}, s_{\bar{q}g}) d\sigma_1(e^+e^- \rightarrow 3 \text{ partons}) + \mathcal{F}], \quad (2.7)$$

where \mathcal{F} is the finite virtual contribution. The dynamical factor \mathcal{K} multiplies the lowest-order three-parton cross section and depends on both s_{\min} and the invariant masses of the hard partons. Combining (2.5) and (2.7) yields the full $O(\alpha_s^2)$ three-jet cross section

$$d\sigma_2(e^+e^- \rightarrow 3 \text{ jets}) = \Theta \left[d\sigma_2^R(e^+e^- \rightarrow 3 \text{ partons}) + \int d\sigma_2^R(e^+e^- \rightarrow 4 \text{ partons}) \right]. \quad (2.8)$$

Formally, (2.5)–(2.7) are evaluated in d dimensions; however, we see that (2.7) is, in fact, finite and the 4-dimensional limit may now be taken. In particular, $d\sigma_1(e^+e^- \rightarrow 3 \text{ partons})$ may be evaluated in 4 dimensions. Furthermore, the resolved four-parton cross section is also finite and one can set $d = 4$ with impunity. It is now straightforward to apply Monte Carlo techniques to numerically estimate the cross section—three- and four-parton events are generated and tested according to the experimental jet definition Θ to see whether or not three physical jets are observed. Note that this approach is closely related to that developed in QED [30]. Recently, a similar cutoff approach to isolate the phase space divergences for initial-state partons has been implemented by Owens and collaborators [31].

III. THE DIVERGENT CONTRIBUTION FROM ONE “UNRESOLVED” PARTON

In the previous sections, we have used the concept of a parton resolution parameter to define finite resolved parton cross sections for $e^+e^- \rightarrow n$ partons at leading and next-to-leading order. In this section, we will first isolate the soft and collinear divergences in the matrix elements and then use the parton resolution criteria to derive the divergent contribution to the cross section when one parton is unresolved. For simplicity, we will work only at leading order in the number of colors. The method is, of course, easily extended to include the subleading terms [32] (for a brief discussion of the subleading color terms for the case of $e^+e^- \rightarrow q\bar{q}g$ see Sec. III J). First of all, we must define some notation.

For e^+e^- collisions at $\sqrt{s} = Q$, the leading-order cross section for n -jet production according to some experimental jet definition Θ contributes at $O(\alpha_s^{n-2})$ and has the form

$$d\sigma_{n-2}(e^+e^- \rightarrow n \text{ jets}) = \Theta d\sigma_{n-2}^R(e^+e^- \rightarrow n \text{ partons}). \quad (3.1)$$

The resolved parton cross section is given by

$$d\sigma_{n-2}^R(e^+e^- \rightarrow n \text{ partons}) = \Phi \left| \mathcal{M}(1, \dots, n) \right|^2 dP^R(Q; 1, \dots, n), \quad (3.2)$$

where the flux factor, $\Phi = 1/8Q^2$, contains the averaging factors over the initial particle spins, $\left| \mathcal{M}(1, \dots, n) \right|^2$ are the leading order matrix elements for n -parton production while the resolved n -body phase space dP^R is evaluated numerically in 4 dimensions with the constraint

that all the partons are resolved according to the parton resolution parameter s_{\min} :

$$dP^R(Q; 1, \dots, n) = \frac{1}{n_g! \prod_f n_q^f! \prod_{f'} n_{\bar{q}}^{f'}!} \times \prod_{ij} \theta(s_{ij} - s_{\min}) dP(Q; 1, \dots, n), \quad (3.3)$$

where the identical particle factor for n_g resolved gluons and n_q^f ($n_{\bar{q}}^{f'}$) resolved quarks (antiquarks) with flavor f has been included. With this choice for the resolved phase space, we define the statistical factor that must be included in the matrix elements due to unresolved partons.

As discussed in Sec. II, the next-to-leading-order n -jet cross section receives contributions from both the next-to-leading n -parton cross section and the lowest-order $(n+1)$ -parton cross section:

$$d\sigma_{n-1}(e^+e^- \rightarrow n \text{ jets}) = \Theta \left[d\sigma_{n-1}^R(e^+e^- \rightarrow n \text{ partons}) + \int d\sigma_{n-1}^R(e^+e^- \rightarrow n+1 \text{ partons}) \right], \quad (3.4)$$

where

$$d\sigma_{n-1}^R(e^+e^- \rightarrow n \text{ partons}) = \Phi \left| \mathcal{M}(1, \dots, n) \right|_F^2 dP^R(Q; 1, \dots, n), \quad (3.5)$$

$$d\sigma_{n-1}^R(e^+e^- \rightarrow n+1 \text{ partons}) = \Phi \left| \mathcal{M}(1, \dots, n+1) \right|^2 dP^R(Q; 1, \dots, n+1).$$

The effective next-to-leading order matrix elements for n -parton production are defined by

$$\left| \mathcal{M}(1, \dots, n) \right|_F^2 = \left| \mathcal{M}(1, \dots, n) \right|_S^2 + \left| \mathcal{M}(1, \dots, n) \right|_C^2 + \left| \mathcal{M}(1, \dots, n) \right|_V^2, \quad (3.6)$$

where subscripts indicate the contributions from the unresolved soft or collinear portions of phase space or from the virtual contributions. We will now derive the structure of $\left| \mathcal{M} \right|_S^2$ and $\left| \mathcal{M} \right|_C^2$.

A. Tree-level matrix elements

The lowest-order matrix element for (1.4) is given by

$$\mathcal{M}(Q_1; 1, \dots, n; \bar{Q}_2) = \widehat{S}_\mu(Q_1; 1, \dots, n; \bar{Q}_2) V^\mu, \quad (3.7)$$

while, for (1.5),

$$\mathcal{M}(Q_1, \bar{Q}_2; Q_3, \bar{Q}_4; 1, \dots, n-2) = \widehat{T}_\mu(Q_1, \bar{Q}_2; Q_3, \bar{Q}_4; 1, \dots, n-2) V^\mu. \quad (3.8)$$

In these expressions, V^μ represents the lepton current, while \widehat{S}_μ and \widehat{T}_μ are currents containing quarks and gluons. These currents depend on the momenta of the partons which we denote by K_1, \dots, K_n for the outgoing gluons and Q_1, Q_3 (\bar{Q}_2, \bar{Q}_4) for the outgoing quarks (antiquarks). Similarly, the gluon color is denoted by a_1, \dots, a_n while that of the quark is c_1, \dots, c_4 . Finally, the flavor of quark (antiquark) is denoted by f_i .

The current \widehat{S}_μ may be decomposed according to the color structure [20, 33, 13]

$$\widehat{S}_\mu(Q_1; 1, \dots, n; \bar{Q}_2) = ieg^n \sum_{P(1, \dots, n)} (T^{a_1} \dots T^{a_n})_{c_1 c_2} S_\mu(Q_1; 1, \dots, n; \bar{Q}_2), \quad (3.9)$$

where $S_\mu(Q_1; 1, \dots, n; \bar{Q}_2)$ represents the colorless subamplitude where the gluons are emitted in an ordered way from the quark line. By summing over all permutations of gluon emission, all Feynman diagrams are accounted for. Note

that the color factor associated with each \mathcal{S}_μ is also ordered according to the color index of the gluon.

Similarly, the four-quark current may be decomposed as

$$\begin{aligned} \widehat{T}_\mu(Q_1, \overline{Q}_2; Q_3, \overline{Q}_4; 1, \dots, n-2) &= \widehat{A}_\mu(Q_1, \overline{Q}_2; Q_3, \overline{Q}_4; 1, \dots, n-2) - \widehat{A}_\mu(Q_1, \overline{Q}_4; Q_3, \overline{Q}_2; 1, \dots, n-2) \\ &\quad + \widehat{A}_\mu(Q_3, \overline{Q}_4; Q_1, \overline{Q}_2; 1, \dots, n-2) - \widehat{A}_\mu(Q_3, \overline{Q}_2; Q_1, \overline{Q}_4; 1, \dots, n-2), \end{aligned} \quad (3.10)$$

where

$$\begin{aligned} &\widehat{A}_\mu(Q_1, \overline{Q}_2; Q_3, \overline{Q}_4; 1, \dots, n-2) \\ &= i \frac{eg^n}{2} \delta_{f_3 f_4} \sum_{P(1, \dots, n-2)} \sum_{i=0}^{n-2} \left[(T^{a_1} \dots T^{a_i})_{c_1 c_4} (T^{a_{i+1}} \dots T^{a_{n-2}})_{c_3 c_2} \mathcal{A}_\mu^{f_1 f_2}(Q_1; 1, \dots, i; \overline{Q}_4 | Q_3; i+1, \dots, n-2; \overline{Q}_2) \right. \\ &\quad \left. - \frac{1}{N} (T^{a_1} \dots T^{a_i})_{c_1 c_2} (T^{a_{i+1}} \dots T^{a_{n-2}})_{c_3 c_4} \right. \\ &\quad \left. \times \mathcal{B}_\mu^{f_1 f_2}(Q_1; 1, \dots, i; \overline{Q}_2 | Q_3; i+1, \dots, n-2; \overline{Q}_4) \right]. \end{aligned} \quad (3.11)$$

This amplitude represents Feynman diagrams where quarks Q_1, \overline{Q}_2 are coupled to the lepton current, while the $Q_3 \overline{Q}_4$ pair is attached via a virtual gluon. Other configurations are obtained by permuting the quarks and antiquarks as in (3.10). By summing over the colors of the internal gluon, two color structures are generated. At leading order in the number of colors, quarks Q_1 and \overline{Q}_4 (and Q_3 and \overline{Q}_2) are color connected and gluons $1, \dots, i$ ($i+1, \dots, n-2$) are emitted in an ordered way from each colored line respectively. This is represented by the ordered subamplitude $\mathcal{A}_\mu^{f_1 f_2}$. The second, color suppressed term is QED like and is described by $\mathcal{B}_\mu^{f_1 f_2}$ where now Q_1 and \overline{Q}_2 (and Q_3 and \overline{Q}_4) are color connected. Summing over i allows any number of gluons to couple to each colored line, and, as before, all permutations of gluon emission are summed over.

B. Squared matrix elements

At leading order in the number of colors, the squared matrix elements for (1.4) are given by

$$\begin{aligned} n=0, \quad &|\widehat{\mathcal{S}}_\mu V^\mu|^2 = e^2 N |\mathcal{S}_\mu V^\mu|^2, \\ n \geq 1, \quad &|\widehat{\mathcal{S}}_\mu V^\mu|^2 = e^2 \left(\frac{g^2 N}{2} \right)^n \left(\frac{N^2 - 1}{N} \right) \left[\sum_{P(1, \dots, n)} |\mathcal{S}_\mu V^\mu|^2 + O\left(\frac{1}{N^2}\right) \right]. \end{aligned} \quad (3.12)$$

Strictly speaking, at leading order in N , we should replace $(N^2 - 1)/N$ by N . However, it is an overall factor, and by including it, we keep all terms to $O(1/N^2)$.

In the four-quark process, (1.5), we may neglect the contribution from $\mathcal{B}_\mu^{f_1 f_2}$, (3.11), at leading order in the number of colors. The squared matrix elements are then given by

$$\begin{aligned} |\widehat{T}_\mu V^\mu|^2 &= e^2 \left(\frac{g^2 N}{2} \right)^n \left(\frac{N^2 - 1}{N^2} \right) \\ &\quad \times \sum_{P(1, \dots, n-2)} \sum_{i=0}^{n-2} \left[|\mathcal{X}_\mu^i(Q_1, \overline{Q}_2; Q_3, \overline{Q}_4) V^\mu|^2 + |\mathcal{X}_\mu^i(Q_1, \overline{Q}_4; Q_3, \overline{Q}_2) V^\mu|^2 + O\left(\frac{1}{N}\right) \right], \end{aligned} \quad (3.13)$$

where,

$$\begin{aligned} \mathcal{X}_\mu^i(Q_1, \overline{Q}_2; Q_3, \overline{Q}_4) &= \mathcal{A}_\mu^{f_1 f_2}(Q_1; 1, \dots, i; \overline{Q}_4 | Q_3; i+1, \dots, n-2; \overline{Q}_2) \\ &\quad + \mathcal{A}_\mu^{f_3 f_4}(Q_3; i+1, \dots, n-2; \overline{Q}_2 | Q_1; 1, \dots, i; \overline{Q}_4). \end{aligned} \quad (3.14)$$

Depending on the flavors of the quarks, not all of these terms will contribute. For example, if pair $Q_1 \overline{Q}_2$ has a different flavor from $Q_3 \overline{Q}_4$, then the second term in (3.13) vanishes according to the flavor δ function in (3.11). It is interesting to note that within the function \mathcal{X} , the order

of gluon emission with respect to the quarks is fixed. This is enforced by the color structure, and, as we will see later, determines the soft gluon behavior of the four-quark matrix elements.

Note that, the two-quark process (3.12) and the four-

quark process (3.13) generate the first two terms $\sigma^{(1)}$ and $\sigma^{(2)}$, respectively, in the color expansion of the $e^+e^- \rightarrow$ jets cross section:

$$\hat{\sigma}_n = N^{n+1} \left[\sigma^{(1)} + \frac{1}{N} \sigma^{(2)} + O\left(\frac{1}{N^2}\right) \right]. \quad (3.15)$$

We see that the terms neglected in the color expansion of the two processes (3.12) and (3.13) are of both $O(1/N^2)$ in the jet cross section. Adding another term in the color expansion involves contributions from the six-quark process, $e^+e^- \rightarrow q\bar{q}q\bar{q}q\bar{q} + (n-4)g$, in addition to the $O(1/N^2)$ terms of (3.12) and the $O(1/N)$ terms of (3.13).

C. The soft behavior of the matrix elements

The soft gluon behavior for an ordered subamplitude is very similar to the soft photon behavior of QED amplitudes. In QED, the soft photon couples to a charged fermion line, resulting in an eikonal factor multiplying the hard process [34]. For example, for a process with n photons (with momenta K_i and polarization vectors ϵ_i , $i = 1, \dots, n$) coupled to a charged fermion pair (with momenta Q and P), the matrix element $\mathcal{M}(Q; 1, \dots, n; P)$ factorizes when photon n becomes soft:

$$\mathcal{M}(Q; 1, \dots, n; P) \rightarrow e e(Q; n; P) \mathcal{M}(Q; 1, \dots, n-1; P), \quad (3.16)$$

where

$$\begin{aligned} \mathcal{S}_\mu(Q_1; 1, \dots, n, s; \bar{Q}_2) &\rightarrow e(n; s; \bar{Q}_2) \mathcal{S}_\mu(Q_1; 1, \dots, n; \bar{Q}_2), \\ \mathcal{S}_\mu(Q_1; 1, \dots, m, s, m+1, \dots, n+1; \bar{Q}_2) &\rightarrow e(m; s; m+1) \mathcal{S}_\mu(Q_1; 1, \dots, n; \bar{Q}_2), \\ \mathcal{S}_\mu(Q_1; s, 1, \dots, n+1; \bar{Q}_2) &\rightarrow e(Q_1; s; 1) \mathcal{S}_\mu(Q_1; 1, \dots, n; \bar{Q}_2), \end{aligned} \quad (3.18)$$

where $e(a; s; b)$ is given by (3.17). It is important to note that in QCD, a and/or b may be either a hard gluon or a quark. Using these relations, the leading color contribution to the squared matrix element for $e^+e^- \rightarrow q\bar{q} + (n+1)g$ with one gluon soft is

$$\left| \widehat{\mathcal{S}}_\mu V^\mu \right|^2 \rightarrow e^2 \left(\frac{g^2 N}{2} \right)^n \left(\frac{N^2 - 1}{N} \right) \sum_{P(1, \dots, n)} \left[s_F(Q_1; 1, \dots, n; \bar{Q}_2) \left| \mathcal{S}_\mu(Q_1; 1, \dots, n; \bar{Q}_2) V^\mu \right|^2 + O\left(\frac{1}{N^2}\right) \right], \quad (3.19)$$

where

$$s_F(Q_1; 1, \dots, n; \bar{Q}_2) = \left(\frac{g^2 N}{2} \right) \left[f_{Q_1 1}(s) + f_{12}(s) + \dots + f_{n \bar{Q}_2}(s) \right], \quad (3.20)$$

and where

$$f_{ab}(s) = \left| e(a; s; b) \right|^2 = \frac{4s_{ab}}{s_{as}s_{sb}}. \quad (3.21)$$

Note that compared to tree level (3.12), each term in the summation is now multiplied by a function s_F which contains all the soft gluon singularities. Furthermore, the soft factor s_F depends on the order of the hard parton momenta and is different for each gluon permutation. Clearly, the squared matrix elements do not exhibit an overall factorization in the soft gluon limit.

Since the gluons are identical, we could have chosen any of the $(n+1)$ gluons to be soft resulting in a factor of $(n+1)$. On the other hand, the identical particle factor (3.3) for the remaining n gluons is $1/n!$ rather than $1/(n+1)!$, so that the factors of $(n+1)$ cancel. The net result is that we can choose one of the gluons to be soft and ignore the identical-particle factors of $(n+1)$.

$$e(Q; n; P) = \epsilon_n^\mu \left(\frac{Q_\mu}{Q \cdot K_n} - \frac{P_\mu}{K_n \cdot P} \right). \quad (3.17)$$

The only Feynman diagrams that contribute in this limit are those where the soft photon couples to the external charged fermion lines.

In QCD, the gluons are themselves colored and there is not an overall factorization of the matrix elements in the soft gluon limit. However, the ordered subamplitudes do exhibit a factorization of the soft gluon singularities as in (3.16) [35, 32]. This is because the partons are ordered and form well defined color charge lines to which the soft gluon can couple [36]. As in the QED case, we obtain an eikonal factor (which may depend on hard gluon momenta) which contains the singular soft behavior. Together with the factorization of multiple soft gluon emission, this was proven in Ref. [32] to which we refer the reader for a more detailed discussion. The soft gluon behavior depends only on the momenta of the external color charged lines to which the soft gluon couples, and is independent of the number and type of other partons in the process. Similarly, the soft factor is independent of whether or not any color singlet particles such as electroweak bosons are participating in the hard scattering.

We will now examine the soft gluon behavior of processes (1.4) and (1.5). If we take gluon s soft, the colorless ordered subamplitude \mathcal{S}_μ (3.9) factorizes into an eikonal factor multiplying the ordered subamplitude for n gluon emission. Depending on the position of the soft gluon with respect to the hard partons, we find

For $e^+e^- \rightarrow q\bar{q}q\bar{q} + (n-1)g$, the derivation of the soft gluon behavior is completely analogous. We find

$$\begin{aligned} |\widehat{T}_\mu V^\mu|^2 &\rightarrow e^2 \left(\frac{g^2 N}{2}\right)^n \left(\frac{N^2-1}{N^2}\right) \\ &\times \sum_{P(1,\dots,n-2)} \sum_{i=0}^{n-2} \left[s_F(Q_1; 1, \dots, i; \bar{Q}_4 | Q_3; i+1, \dots, n-2; \bar{Q}_2) \left| \mathcal{X}_\mu^i(Q_1, \bar{Q}_2; Q_3, \bar{Q}_4) V^\mu \right|^2 \right. \\ &\quad \left. + s_F(Q_1; 1, \dots, i; \bar{Q}_2 | Q_3; i+1, \dots, n-2; \bar{Q}_4) \left| \mathcal{X}_\mu^i(Q_1, \bar{Q}_4; Q_3, \bar{Q}_2) V^\mu \right|^2 + O\left(\frac{1}{N}\right) \right], \end{aligned} \quad (3.22)$$

where, because the order of gluon emission with respect to the quarks within \mathcal{X} is fixed,

$$\begin{aligned} s_F(Q_1; 1, \dots, i; \bar{Q}_4 | Q_3; i+1, \dots, n-2; \bar{Q}_2) \\ &= s_F(Q_3; i+1, \dots, n-2; \bar{Q}_2 | Q_1; 1, \dots, i; \bar{Q}_4) \\ &= \left(\frac{g^2 N}{2}\right) \left[f_{Q_1 1}(s) + f_{12}(s) + \dots + f_{i\bar{Q}_4}(s) + f_{Q_3 i+1}(s) + \dots + f_{n-2\bar{Q}_2}(s) \right] \\ &= s_F(Q_1; 1, \dots, i; \bar{Q}_4) + s_F(Q_3; i+1, \dots, n-2; \bar{Q}_2). \end{aligned} \quad (3.23)$$

As before, we obtain a structure where each term in the sum over gluon permutations is tree level (3.13) multiplied by a permutation-dependent function containing the soft gluon singularities.

D. The soft behavior of phase space

Having isolated the soft behavior of the matrix elements, we need also to derive the soft behavior of $(n+1)$ -particle phase space in d dimensions. As we will show, the phase space factorizes into an n -particle phase space multiplied by an integral over the soft momenta. In d dimensions, n -particle phase space of a particle with mass $\sqrt{Q^2}$ decaying into n massless particles with momenta \mathbf{P}_i and energy E_i is given by

$$\begin{aligned} dP^d(Q; P_1, \dots, P_n) &= \left[\prod_{i=1}^n \frac{d^{d-1}\mathbf{P}_i}{(2\pi)^{d-1} 2E_i} \right] (2\pi)^d \delta^{(d)}(Q - P_1 - \dots - P_n) \\ &= (2\pi)^{n-d(n-1)} dR^d(Q; P_1, \dots, P_n). \end{aligned} \quad (3.24)$$

For example, the two-body phase space factor dR is given by

$$dR^d(Q; P_1, P_2) = s_{12}^{\frac{d-4}{2}} \frac{d\Omega_{d-1}}{2^{d-1}} ds_{12} \delta(s_{12} - Q^2), \quad (3.25)$$

where we have transformed the integration variables to an integration over the two-particle invariant mass s_{12} and the $(d-1)$ -dimensional orientation angle.

Similarly, the three-particle phase space is

$$dR^d(Q; P_1, P_2, P_3) = \frac{\pi^{\frac{d-2}{2}}}{2\Gamma(\frac{d-2}{2})} (Q^2)^{\frac{2-d}{2}} \left[s_{12} s_{13} s_{23} \right]^{\frac{d-4}{2}} \frac{d\Omega_{d-1}}{2^{d-1}} ds_{12} ds_{13} ds_{23} \delta(s_{12} + s_{13} + s_{23} - Q^2). \quad (3.26)$$

Since we will take momentum P_3 to be unresolved, we have integrated out the angular orientation of P_3 with respect to the observed momenta P_1 and P_2 . We define the region when P_3 is soft to be

$$s_{i3} < s_{\min} \ll Q^2 \quad (i = 1, 2), \quad (3.27)$$

where s_{\min} is the parton resolution parameter discussed in Sec. II. In this limit, we ignore momentum P_3 in the numerator of (3.26) and the three-body phase space factorizes:

$$dR^d(Q; P_1, P_2, P_3) \rightarrow dR^d(Q; P_1, P_2) dR_{\text{soft}}^d(P_1, P_2, P_3), \quad (3.28)$$

where

$$dR_{\text{soft}}^d(P_1, P_2, P_3) = \frac{\pi^{\frac{d-2}{2}}}{2\Gamma(\frac{d-2}{2})} s_{12}^{\frac{2-d}{2}} ds_{13} ds_{23} \left[s_{13} s_{23} \right]^{\frac{d-4}{2}} \theta(s_{\min} - s_{13}) \theta(s_{\min} - s_{23}). \quad (3.29)$$

Specializing to the case $d = 4 - 2\epsilon$, the soft phase space factor is

$$dP_{\text{soft}}^\epsilon(P_1, P_2, P_3) = \frac{(4\pi)^\epsilon}{16\pi^2\Gamma(1-\epsilon)} \frac{ds_{13}ds_{23}}{s_{12}} \left[\frac{s_{13}s_{23}}{s_{12}} \right]^{-\epsilon} \theta(s_{\min} - s_{13})\theta(s_{\min} - s_{23}). \quad (3.30)$$

It is straightforward to generalize this factorization for $(n+1)$ -particle phase space by splitting off a three-body phase space, taking the soft limit and then recombining the resulting two-body phase space. For example, when P_s becomes soft, we have

$$\begin{aligned} dR^d(Q; P_1, \dots, P_{n-2}, P_a, P_b, P_s) &= dR^d(Q; P_1, \dots, P_{n-2}, P_H) dP_H^2 dR^d(P_H; P_a, P_b, P_s) \\ &\rightarrow dR^d(Q; P_1, \dots, P_{n-2}, P_H) dP_H^2 dR^d(P_H; P_a, P_b) dR_{\text{soft}}^d(P_a, P_b, P_s) \\ &= dR^d(Q; P_1, \dots, P_{n-2}, P_a, P_b) dR_{\text{soft}}^d(P_a, P_b, P_s). \end{aligned} \quad (3.31)$$

We can therefore always factor out a soft phase space factor associated with the unresolved gluon which regularizes matrix element singularities in s_{as} and s_{sb} . As can be seen in (3.20) and (3.23), the matrix elements never have overlapping divergences with more than two singular invariant masses. Therefore, by suitably factorizing the soft phase space for each ordered subamplitude we obtain a completely regular cross section.

E. The soft behavior of the cross section

In the previous subsections, we have shown how the matrix elements and phase space factorize when one of the gluons become soft. We will now combine these results to obtain the soft behavior of the cross section for $e^+e^- \rightarrow q\bar{q} + (n+1)g$ and $e^+e^- \rightarrow q\bar{q}q\bar{q} + (n-1)g$. Omitting the overall flux Φ in the intermediate steps, the cross section contribution from a single ordered subamplitude, \mathcal{S}_μ , when gluon s is soft is

$$\begin{aligned} d\sigma_{n+1} &= \left| \mathcal{S}_\mu(Q_1; 1, \dots, a, s, b, \dots, n; \bar{Q}_2) V^\mu \right|^2 dP^d(Q; Q_1, \bar{Q}_2, 1, \dots, a, b, s) \\ &\rightarrow \left(\frac{g^2 N}{2} \right) f_{ab}(s) dP_{\text{soft}}^\epsilon(a, b, s) \left| \mathcal{S}_\mu(Q_1; 1, \dots, n; \bar{Q}_2) V^\mu \right|^2 dP^d(Q; Q_1, \bar{Q}_2, 1, \dots, n) \\ &= \left[\left(\frac{g^2 N}{2} \right) f_{ab}(s) dP_{\text{soft}}^\epsilon(a, b, s) \right] d\sigma_n. \end{aligned} \quad (3.32)$$

All of the dependence on the soft gluon momenta has factorized and multiplies the cross section for a single ordered subamplitude for $e^+e^- \rightarrow q\bar{q} + ng$ where now all the partons are resolved. We can now integrate out the soft gluon behavior for this subamplitude using (3.21) and (3.30) and leaving all other phase space integrations over the resolved partons undone:

$$\begin{aligned} \int \left(\frac{g^2 N}{2} \right) f_{ab}(s) dP_{\text{soft}}^\epsilon(a, b, s) &= \left(\frac{\alpha_s N}{2\pi} \right) \frac{(4\pi\mu^2)^\epsilon}{\Gamma(1-\epsilon)} \frac{1}{s_{ab}} \int_0^{s_{\min}} ds_{as} \int_0^{s_{\min}} ds_{sb} \left[\frac{s_{as}s_{sb}}{s_{ab}} \right]^{-1-\epsilon} \\ &= \left(\frac{\alpha_s N}{2\pi} \right) \frac{1}{\Gamma(1-\epsilon)} \left(\frac{4\pi\mu^2}{s_{\min}} \right)^\epsilon \frac{1}{\epsilon^2} \left(\frac{s_{ab}}{s_{\min}} \right)^\epsilon, \end{aligned} \quad (3.33)$$

where μ is an arbitrary scale introduced to keep the strong coupling constant, $\alpha_s = g^2\mu^{-2\epsilon}/4\pi$, dimensionless in d dimensions.

By choosing the correct soft phase space factor to integrate for each subamplitude, this procedure can be extended to include the full soft behavior of the cross section:

$$S_F(Q_1; 1, \dots, n; \bar{Q}_2) = \left(\frac{\alpha_s N}{2\pi} \right) \frac{1}{\Gamma(1-\epsilon)} \left(\frac{4\pi\mu^2}{s_{\min}} \right)^\epsilon \frac{1}{\epsilon^2} \left[\left(\frac{s_{Q_1 1}}{s_{\min}} \right)^\epsilon + \left(\frac{s_{12}}{s_{\min}} \right)^\epsilon + \dots + \left(\frac{s_{n\bar{Q}_2}}{s_{\min}} \right)^\epsilon \right]. \quad (3.34)$$

Note that this factor is dependent on the gluon permutation and multiplies the cross section for each ordered subamplitude. At leading order in the number of colors, the effective squared matrix elements for $e^+e^- \rightarrow q\bar{q} + ng$ with one unresolved soft gluon are, therefore,

$$\left| \widehat{S}_\mu V^\mu \right|_S^2 = e^2 \left(\frac{g^2 N}{2} \right)^n \left(\frac{N^2 - 1}{N} \right) \sum_{P(1, \dots, n)} \left[S_F(Q_1; 1, \dots, n; \bar{Q}_2) \left| \mathcal{S}_\mu(Q_1; 1, \dots, n; \bar{Q}_2) V^\mu \right|^2 + O\left(\frac{1}{N^2} \right) \right]. \quad (3.35)$$

As discussed in Sec. III J, the subleading color terms have a similar structure, see (3.83)–(3.85).

Similarly, the soft behavior of the cross section for $e^+e^- \rightarrow q\bar{q}q\bar{q} + (n-2)g$ is obtained by integrating out the soft gluon in (3.22) to yield

$$\begin{aligned}
|\widehat{T}_\mu V^\mu|_S^2 &= e^2 \left(\frac{g^2 N}{2} \right)^n \left(\frac{N^2 - 1}{N^2} \right) \\
&\times \sum_{P(1, \dots, n-2)} \sum_{i=0}^{n-2} \left[S_F(Q_1; 1, \dots, i; \overline{Q}_4 | Q_3; i+1, \dots, n-2; \overline{Q}_2) \left| \mathcal{X}_\mu^i(Q_1, \overline{Q}_2; Q_3, \overline{Q}_4) V^\mu \right|^2 \right. \\
&\quad \left. + S_F(Q_1; 1, \dots, i; \overline{Q}_2 | Q_3; i+1, \dots, n-2; \overline{Q}_4) \left| \mathcal{X}_\mu^i(Q_1, \overline{Q}_4; Q_3, \overline{Q}_2) V^\mu \right|^2 + O\left(\frac{1}{N}\right) \right], \tag{3.36}
\end{aligned}$$

where

$$S_F(Q_1; 1, \dots, i; \overline{Q}_4 | Q_3; i+1, \dots, n-2; \overline{Q}_2) = S_F(Q_1; 1, \dots, i; \overline{Q}_4) + S_F(Q_3; i+1, \dots, n-2; \overline{Q}_2). \tag{3.37}$$

F. The collinear behavior of the matrix elements

In addition to being singular in the soft gluon region, the matrix elements are also singular when partons a and b become collinear and cluster to form a new parton c such that

$$P_a + P_b = P_c. \tag{3.38}$$

Unlike the soft gluon case, the matrix elements exhibit an overall factorization in the collinear limit,

$$|\mathcal{M}(\dots, a, b, \dots)|^2 \rightarrow \hat{c}_F^{ab \rightarrow c} |\mathcal{M}(\dots, c, \dots)|^2, \tag{3.39}$$

where the collinear factor $\hat{c}_F^{ab \rightarrow c}$ is defined by (3.39) and is singular as $s_{ab} \rightarrow 0$. Removing the parton-dependent color factor,

$$\begin{aligned}
\hat{c}_F^{gg \rightarrow g} &= \left(\frac{g^2 N}{2} \right) f^{gg \rightarrow g}, \\
\hat{c}_F^{gg \rightarrow q} &= \left(\frac{g^2 N}{2} \right) \left(1 - \frac{1}{N^2} \right) f^{gg \rightarrow q}, \\
\hat{c}_F^{q\bar{q} \rightarrow g} &= \left(\frac{g^2 n_f}{2} \right) f^{q\bar{q} \rightarrow g},
\end{aligned} \tag{3.40}$$

yields the color-reduced collinear factor

$$f^{ab \rightarrow c} = \frac{1}{s_{ab}} P_{ab \rightarrow c}(z). \tag{3.41}$$

Note that in the $gg \rightarrow g$ case, a factor of $1/2!$ is included because the gluons are identical. In deriving (3.39)–(3.41), we have implicitly averaged over the azimuthal angle of a and b relative to c . This suppresses spurious angular correlations between unresolved partons. The function $P_{ab \rightarrow c}(z)$ is trivially related to the Altarelli-Parisi splitting function [37] in d -dimensions for partons a and b with momentum fraction z clustering to form parton c , such that

$$P_a = zP_c, \quad P_b = (1-z)P_c. \tag{3.42}$$

The Altarelli-Parisi splitting functions are symmetric un-

der the exchanges $a \leftrightarrow b$, $z \leftrightarrow (1-z)$,

$$P_{ab \rightarrow c}(z) = P_{ba \rightarrow c}(1-z), \tag{3.43}$$

and, under charge conjugation,

$$P_{a\bar{b} \rightarrow \bar{c}}(z) = P_{ab \rightarrow c}(z), \tag{3.44}$$

so that there are only three independent splitting functions: $P_{gg \rightarrow g}$, $P_{qg \rightarrow q}$, and $P_{q\bar{q} \rightarrow g}$. In defining these functions, there is some scheme dependence since one can treat the hard parton c in either d or 4 dimensions. (The collinear partons are, of course, strictly d dimensional to regulate the collinear singularities.) The first scheme is the conventional prescription for QCD higher-order corrections where all particles are taken in d -dimensions, while the second follows the 't Hooft-Veltman philosophy [21] of keeping observable particles in 4-dimensions. In the conventional scheme, the splitting functions are given by

$$\begin{aligned}
P_{gg \rightarrow g}(z) &= 2 \left(\frac{1+z^4+(1-z)^4}{z(1-z)} \right), \\
P_{qg \rightarrow q}(z) &= 2 \left(\frac{1+z^2-\epsilon(1-z)^2}{1-z} \right), \\
P_{q\bar{q} \rightarrow g}(z) &= 2 \left(\frac{z^2+(1-z)^2-\epsilon}{1-\epsilon} \right).
\end{aligned} \tag{3.45}$$

The 't Hooft-Veltman splitting functions differ from these by terms of order ϵ :

$$\begin{aligned}
P_{gg \rightarrow g}^{HV}(z) &= P_{gg \rightarrow g}(z) - 4\epsilon z(1-z), \\
P_{qg \rightarrow q}^{HV}(z) &= P_{qg \rightarrow q}(z), \\
P_{q\bar{q} \rightarrow g}^{HV}(z) &= (1-\epsilon)P_{q\bar{q} \rightarrow g}(z) + 2\epsilon.
\end{aligned} \tag{3.46}$$

Since the collinear pole is $O(1/\epsilon)$, this will lead to different constant terms in the total n -parton cross section.

The behavior of the ordered subamplitudes for $e^+e^- \rightarrow q\bar{q} + (n+1)g$ in the collinear limit is quite straightforward. First of all, there is only a singular contribution when the collinear partons are adjacent. For example, if two adjacent gluons are collinear and form gluon m then

$$\left| \mathcal{S}_\mu(Q_1; 1, \dots, m-1, g, g, m+1, \dots, n; \overline{Q}_2) V^\mu \right|^2 \rightarrow f^{gg \rightarrow m} \left| \mathcal{S}_\mu(Q_1; 1, \dots, m-1, m, m+1, \dots, n; \overline{Q}_2) V^\mu \right|^2. \quad (3.47)$$

Similarly, there is a contribution when one of the gluons is collinear with either the quark or antiquark:

$$\begin{aligned} \left| \mathcal{S}_\mu(q; g, 1, \dots, n; \overline{Q}_2) V^\mu \right|^2 &\rightarrow f^{qg \rightarrow Q_1} \left| \mathcal{S}_\mu(Q_1; 1, \dots, n; \overline{Q}_2) V^\mu \right|^2, \\ \left| \mathcal{S}_\mu(Q_1; 1, \dots, n, g; \overline{q}) V^\mu \right|^2 &\rightarrow f^{g\overline{q} \rightarrow \overline{Q}_2} \left| \mathcal{S}_\mu(Q_1; 1, \dots, n; \overline{Q}_2) V^\mu \right|^2. \end{aligned} \quad (3.48)$$

On the other hand, if the two collinear partons a and b are not adjacent in the ordered subamplitude, there is no singular contribution:

$$\left| \mathcal{S}_\mu(\dots, a, \dots, b, \dots) V^\mu \right|^2 \rightarrow 0. \quad (3.49)$$

In particular, there is no contribution when the quark-antiquark pair is collinear.

However, the four-quark current $e^+e^- \rightarrow q\overline{q}q\overline{q} + (n-1)g$ is singular when a flavor-singlet quark-antiquark pair becomes collinear. For example, if Q_3 and \overline{Q}_4 are collinear and form gluon j , then, keeping only terms that are singular, a two-quark current results:

$$\begin{aligned} \left| \mathcal{X}_\mu^i(Q_1, \overline{Q}_2; Q_3, \overline{Q}_4) V^\mu \right|^2 &\rightarrow f^{Q_3\overline{Q}_4 \rightarrow j} \left| \mathcal{S}_\mu(Q_1; 1, \dots, i, j, i+1, \dots, n-1; \overline{Q}_2) V^\mu \right|^2, \\ \left| \mathcal{X}_\mu^i(Q_1, \overline{Q}_4; Q_3, \overline{Q}_2) V^\mu \right|^2 &\rightarrow 0. \end{aligned} \quad (3.50)$$

In this limit, the full matrix elements squared summed over the n_f flavors of the collinear quark-antiquark pair yield a contribution to the two quark matrix elements at next-to-leading order in the number of colors of

$$\left| \widehat{\mathcal{T}}_\mu V^\mu \right|^2 \rightarrow e^2 \left(\frac{g^2 N}{2} \right)^n \left(\frac{N^2 - 1}{N} \right) \sum_{P(1, \dots, n)} \left[\left(\frac{g^2 n_f}{2} \right) f^{Q_3\overline{Q}_4 \rightarrow j} \left| \mathcal{S}_\mu(Q_1; 1, \dots, n; \overline{Q}_2) V^\mu \right|^2 + \mathcal{O}\left(\frac{1}{N}\right) \right], \quad (3.51)$$

where the sum over i has been absorbed into the sum over gluon permutations which now extends up to n .

Summing over all possible collinear combinations, we find that the leading and next-to-leading color contribution to the full squared matrix element for the two-quark final state when two partons are collinear is, therefore,

$$\left| \widehat{\mathcal{S}}_\mu V^\mu \right|^2 + \left| \widehat{\mathcal{T}}_\mu V^\mu \right|^2 \rightarrow e^2 \left(\frac{g^2 N}{2} \right)^n \left(\frac{N^2 - 1}{N} \right) \sum_{P(1, \dots, n)} \left[c_F(Q_1; 1, \dots, n; \overline{Q}_2) \left| \mathcal{S}_\mu(Q_1; 1, \dots, n; \overline{Q}_2) V^\mu \right|^2 + \mathcal{O}\left(\frac{1}{N^2}\right) \right], \quad (3.52)$$

where

$$c_F(Q_1; 1, \dots, n; \overline{Q}_2) = \left(\frac{g^2 N}{2} \right) \left[f^{qg \rightarrow Q_1} + f^{gg \rightarrow 1} + \dots + f^{g\overline{q} \rightarrow \overline{Q}_2} + \hat{n}_f n_f f^{q\overline{q} \rightarrow g} \right], \quad (3.53)$$

and

$$\hat{n}_f = \frac{n_f}{N}. \quad (3.54)$$

Note that this is exactly the same structure as that obtained in the soft gluon limit (3.19) and (3.20) and is similar to tree level (3.12), where each term in the sum over gluon permutations is now multiplied by an ordered collinear factor c_F containing all the collinear singularities.

As in the soft gluon case, since all gluons are identical, we could have chosen any gluon to be collinear resulting in an additional factor of $n+1$. However, the identical particle factor (3.3) again cancels this factor and we can just treat one gluon as collinear. On the other hand, when two quarks become collinear the identical particle factor for gluons changes from $1/(n-1)!$ to $1/n!$ leading to the factor of n in (3.53).

For the four-quark final state (1.5) we find a very similar structure:

$$\begin{aligned} \left| \widehat{\mathcal{T}}_\mu V^\mu \right|^2 &\rightarrow e^2 \left(\frac{g^2 N}{2} \right)^n \left(\frac{N^2 - 1}{N^2} \right) \\ &\times \sum_{P(1, \dots, n-2)} \sum_{i=0}^{n-2} \left[c_F(Q_1; 1, \dots, i; \overline{Q}_4 | Q_3; i+1, \dots, n-2; \overline{Q}_2) \left| \mathcal{X}_\mu^i(Q_1, \overline{Q}_2; Q_3, \overline{Q}_4) V^\mu \right|^2 \right. \\ &\quad \left. + c_F(Q_1; 1, \dots, i; \overline{Q}_2 | Q_3; i+1, \dots, n-2; \overline{Q}_4) \left| \mathcal{X}_\mu^i(Q_1, \overline{Q}_4; Q_3, \overline{Q}_2) V^\mu \right|^2 + \mathcal{O}\left(\frac{1}{N}\right) \right], \end{aligned} \quad (3.55)$$

with

$$\begin{aligned}
c_F(Q_1; 1, \dots, i; \overline{Q}_4 | Q_3; i+1, \dots, n-2; \overline{Q}_2) &= c_F(Q_3; i+1, \dots, n-2; \overline{Q}_2 | Q_1; 1, \dots, i+1; \overline{Q}_4) \\
&= \frac{g^2 N}{2} \left[f^{qg \rightarrow Q_1} + f^{gg \rightarrow 1} + \dots + f^{g\bar{q} \rightarrow \overline{Q}_4} + \hat{n}_f f^{q\bar{q} \rightarrow g} \right. \\
&\quad \left. + f^{qg \rightarrow Q_3} + f^{gg \rightarrow i+1} + \dots + f^{g\bar{q} \rightarrow \overline{Q}_2} + \hat{n}_f (n-2-i) f^{q\bar{q} \rightarrow g} \right] \\
&= c_F(Q_1; 1, \dots, i; \overline{Q}_4) + c_F(Q_3; i+1, \dots, n-2; \overline{Q}_2). \tag{3.56}
\end{aligned}$$

Note that the \hat{n}_f terms appearing in (3.56) are generated by the six-quark process $e^+e^- \rightarrow q\bar{q}q\bar{q}q\bar{q} + (n-3)$, when two of the quarks are collinear and form a gluon. The first (second) term proportional to \hat{n}_f is generated when the extra $q\bar{q}$ pair is attached to the color charged line joining Q_1 and \overline{Q}_4 (Q_3 and \overline{Q}_2). Strictly speaking, these terms are subleading in the number of colors and could be neglected (3.15).

G. The collinear behavior of phase space

Having isolated the collinear singularities in the matrix elements, we now need to obtain the collinear behavior of the $(n+1)$ -particle phase space in d dimensions. In particular, we will derive a phase space factorization into an n -particle phase space and a collinear phase space factor which will regulate the collinear poles. We start with 3-particle phase space for $Q \rightarrow P_1 + P_a + P_b$ where P_a and P_b will be collinear and form momenta $P_2 = P_a + P_b$, and integrate out the azimuthal angle between the plane containing P_a and P_b relative to P_2 :

$$dR^d(Q; P_1, P_a, P_b) = \frac{\pi^{\frac{d-2}{2}}}{2\Gamma(\frac{d-2}{2})} (Q^2)^{\frac{2-d}{2}} \left[s_{1a} s_{ab} s_{b1} \right]^{\frac{d-4}{2}} \frac{d\Omega_{d-1}}{2^{d-1}} ds_{1a} ds_{ab} ds_{b1} \delta(s_{1a} + s_{ab} + s_{b1} - Q^2). \tag{3.57}$$

In the collinear region defined by

$$s_{ab} < s_{\min} \ll Q^2, \tag{3.58}$$

we can ignore terms of order s_{ab} and find

$$s_{12} = s_{1a} + s_{b1}. \tag{3.59}$$

We therefore choose to define z by

$$s_{1a} = z s_{12}, \quad s_{b1} = (1-z) s_{12}. \tag{3.60}$$

Note that in the exact collinear limit, this leads to the usual definition of z , (3.42). In this limit, the three-particle phase space factorizes:

$$dR^d(Q; P_1, P_a, P_b) \rightarrow dR^d(Q; P_1, P_2) dR_{\text{col}}^d(P_a, P_b; z), \tag{3.61}$$

where

$$dR_{\text{col}}^d(P_a, P_b; z) = \frac{\pi^{\frac{d-2}{2}}}{2\Gamma(\frac{d-2}{2})} ds_{ab} dz \left[s_{ab} z (1-z) \right]^{\frac{d-4}{2}} \theta(s_{\min} - s_{ab}). \tag{3.62}$$

Choosing $d = 4 - 2\epsilon$ yields the collinear phase space factor

$$dP_{\text{col}}^\epsilon(P_a, P_b; z) = \frac{(4\pi)^\epsilon}{16\pi^2 \Gamma(1-\epsilon)} ds_{ab} dz \left[s_{ab} z (1-z) \right]^{-\epsilon} \theta(s_{\min} - s_{ab}). \tag{3.63}$$

The generalization to $(n+1)$ -particle phase space is again straightforward. Taking $P_a + P_b \rightarrow P_n$, we have

$$\begin{aligned}
dR^d(Q; P_1, \dots, P_{n-1}, P_a, P_b) &= dR^d(Q; P_1, \dots, P_{n-2}, P_H) dP_H^2 dR^d(P_H; P_{n-1}, P_a, P_b) \\
&\rightarrow dR^d(Q; P_1, \dots, P_{n-2}, P_H) dP_H^2 dR^d(P_H; P_{n-1}, P_n) dR_{\text{col}}^d(P_a, P_b; z) = dR^d(Q; P_1, \dots, P_n) dR_{\text{col}}^d(P_a, P_b; z). \tag{3.64}
\end{aligned}$$

As in the soft limit, we can always factor out a collinear phase space factor associated with the unresolved two-parton cluster which regulates the matrix element singularities in s_{ab} (3.41) and z (3.45).

H. The collinear behavior of the cross section

In order to determine the collinear contribution to the cross section, we must integrate out the unresolved parton so that the collinear region does not overlap with the soft region; we must match the collinear region precisely on to the soft region so that there is no double counting and that no singular region is omitted. In other words, we must ensure that only one $s_{ij} < s_{\min}$ and that all other invariant masses are larger than s_{\min} . In general, this is a very complicated constraint, however, using the ordered subamplitudes resolves this problem.

If we consider the clustering of partons a and b , we must ensure that the resulting parton c is resolved from the other partons in the event. This requirement will avoid the soft region and determine the upper and lower integration boundary for z . To see how this works, let us consider a general ordered subamplitude which has the structure

$$\left| \mathcal{S}_\mu(\dots, a-1, a, b, b+1, \dots, d, \dots) V^\mu \right|^2 \sim \frac{1}{s_{a-1a} s_{ab} s_{bb+1}}. \quad (3.65)$$

If the collinear pole is given by $s_{ab} < s_{\min}$, then we can fall into the soft region when either $s_{a-1a} < s_{\min}$ (corresponding to parton a being soft) or $s_{bb+1} < s_{\min}$ (parton b soft). The collinear region is therefore determined by

$$\begin{aligned} \int \left(\frac{g^2 N}{2} \right) f^{ab \rightarrow c}(z_1, z_2) dP_{\text{col}}^\epsilon(P_a, P_b; z) &= \left(\frac{\alpha_s N}{2\pi} \right) \frac{(4\pi\mu^2)^\epsilon}{\Gamma(1-\epsilon)} \int_0^{s_{\min}} ds_{ab} s_{ab}^{-1-\epsilon} \left[\frac{1}{4} \int_{z_1}^{1-z_2} dz [z(1-z)]^{-\epsilon} P_{ab \rightarrow c}(z) \right] \\ &= - \left(\frac{\alpha_s N}{2\pi} \right) \frac{1}{\Gamma(1-\epsilon)} \left(\frac{4\pi\mu^2}{s_{\min}} \right)^\epsilon \frac{1}{\epsilon} I_{ab \rightarrow c}(z_1, z_2). \end{aligned} \quad (3.69)$$

In the conventional scheme, the integrals over the splitting functions, I , are given by

$$\begin{aligned} I_{gg \rightarrow g}(z_1, z_2) &= \frac{z_1^{-\epsilon}}{\epsilon} + \frac{z_2^{-\epsilon}}{\epsilon} - \frac{3(1-\epsilon)(4-3\epsilon)}{2\epsilon(3-2\epsilon)} \frac{\Gamma^2(1-\epsilon)}{\Gamma(2-2\epsilon)} \\ &= \left(\frac{z_1^{-\epsilon} + z_2^{-\epsilon} - 2}{\epsilon} \right) - \frac{11}{6} + \left(-\frac{67}{18} + \frac{\pi^2}{3} \right) \epsilon + O(\epsilon^2), \\ I_{qg \rightarrow q}(z_1, z_2) &= \frac{z_2^{-\epsilon}}{\epsilon} - \frac{(1-\epsilon)(4-\epsilon)}{4\epsilon} \frac{\Gamma^2(1-\epsilon)}{\Gamma(2-2\epsilon)} \\ &= \left(\frac{z_2^{-\epsilon} - 1}{\epsilon} \right) - \frac{3}{4} + \left(-\frac{7}{4} + \frac{\pi^2}{6} \right) \epsilon + O(\epsilon^2), \\ I_{q\bar{q} \rightarrow g}(z_1, z_2) &= \frac{1-\epsilon}{3-2\epsilon} \frac{\Gamma^2(1-\epsilon)}{\Gamma(2-2\epsilon)} \\ &= \frac{1}{3} + \frac{5\epsilon}{9} + O(\epsilon^2), \end{aligned} \quad (3.70)$$

where, since $z_1, z_2 \propto s_{\min}$ we have neglected terms of $O(z_1)$ and $O(z_2)$. Note that I is finite as $\epsilon \rightarrow 0$.

These integrals I are directly related to the Altarelli-Parisi splitting functions, so we also have the relations

$$I_{gq \rightarrow q}(z_1, z_2) = I_{qg \rightarrow q}(z_2, z_1), \quad I_{q\bar{q} \rightarrow g}(z_1, z_2) = I_{q\bar{q} \rightarrow g}(z_2, z_1), \quad (3.71)$$

$$s_{a-1a} = z s_{a-1c} > s_{\min}, \quad (3.66)$$

$$s_{bb+1} = (1-z) s_{cb+1} > s_{\min},$$

where we have used $P_a = z P_c$ and $P_b = (1-z) P_c$. In other words,

$$\frac{s_{\min}}{s_{a-1c}} = z_1 < z < 1 - z_2 = 1 - \frac{s_{\min}}{s_{cb+1}}. \quad (3.67)$$

With this ordering dependent boundary, we neatly match onto the soft region. On the other hand, this does not force c to be resolved from other non-neighboring partons, such as parton d . However, the ordered subamplitude does not contain poles in s_{cd} and the relative error induced by such ‘‘accidental’’ overlaps is of order s_{\min} and therefore negligible.

As in the soft gluon case, (3.32), the contribution to the cross section at leading order in the number of colors from a single ordered subamplitude in the collinear limit is

$$d\sigma_{n+1} = \left[\left(\frac{g^2 N}{2} \right) f^{ab \rightarrow c}(z_1, z_2) dP_{\text{col}}^\epsilon(P_a, P_b; z) \right] d\sigma_n, \quad (3.68)$$

where the z integration boundary, $z_1 < z < 1 - z_2$, has been made explicit. All of the dependence on the unresolved collinear partons has been factorized and multiplies the cross section for a single ordered subamplitude where now all the partons are resolved. We can now integrate out the collinear behavior for this subamplitude using (3.41) and (3.63) and leave all other phase space integrations over the resolved partons undone:

and

$$I_{qg \rightarrow \bar{q}}(z_1, z_2) = I_{qg \rightarrow q}(z_1, z_2), \quad I_{g\bar{q} \rightarrow \bar{q}}(z_1, z_2) = I_{gq \rightarrow q}(z_1, z_2). \quad (3.72)$$

The divergences of the splitting functions are reflected in the behavior of the integrals with respect to z_1 and z_2 . For example, the $qg \rightarrow q$ splitting function is finite when the gluon carries off all of the momentum ($z \rightarrow 0$) but diverges when the gluon is soft ($z \rightarrow 1$). Therefore, $I_{qg \rightarrow q}(z_1, z_2)$ depends logarithmically on z_2 but not on z_1 . Similarly, the $gg \rightarrow g$ integral depends on both z_1 and z_2 while that for $q\bar{q} \rightarrow g$ depends on neither.

By choosing the correct collinear phase space factor to integrate for each subamplitude, this can be extended to include the full collinear behavior of the cross section:

$$\begin{aligned} C_F(Q_1; 1, \dots, n; \bar{Q}_2) &= - \left(\frac{\alpha_s N}{2\pi} \right) \frac{1}{\Gamma(1-\epsilon)} \left(\frac{4\pi\mu^2}{s_{\min}} \right)^\epsilon \frac{1}{\epsilon} \\ &\times \left[I_{qg \rightarrow Q_1} \left(0, \frac{s_{\min}}{s_{Q_1 1}} \right) + I_{gg \rightarrow 1} \left(\frac{s_{\min}}{s_{Q_1 1}}, \frac{s_{\min}}{s_{12}} \right) + \dots + I_{g\bar{q} \rightarrow \bar{Q}_2} \left(\frac{s_{\min}}{s_{n\bar{Q}_2}}, 0 \right) + n\hat{n}_f I_{q\bar{q} \rightarrow g}(0, 0) \right] \\ &= \left(\frac{\alpha_s N}{2\pi} \right) \frac{1}{\Gamma(1-\epsilon)} \left(\frac{4\pi\mu^2}{s_{\min}} \right)^\epsilon \frac{1}{\epsilon^2} \\ &\times \left[-2 \left[\left(\frac{s_{Q_1 1}}{s_{\min}} \right)^\epsilon + \left(\frac{s_{12}}{s_{\min}} \right)^\epsilon + \dots + \left(\frac{s_{n\bar{Q}_2}}{s_{\min}} \right)^\epsilon \right] \right. \\ &\quad \left. + \frac{1-\epsilon}{2(3-2\epsilon)} [12(n+1) - (9n+11+2n\hat{n}_f)\epsilon + 2\epsilon^2] \frac{\Gamma^2(1-\epsilon)}{\Gamma(2-2\epsilon)} \right]. \end{aligned} \quad (3.73)$$

In this equation, the trivial z integration boundaries have been replaced by 0. Note that this factor is dependent on the gluon permutation and multiplies the cross section for each ordered subamplitude. The effective squared matrix elements for $e^+e^- \rightarrow q\bar{q} + ng$ with an unresolved collinear pair are, therefore,

$$|\widehat{S}_\mu V^\mu|_C^2 = e^2 \left(\frac{g^2 N}{2} \right)^n \left(\frac{N^2 - 1}{N} \right) \sum_{P(1, \dots, n)} \left[C_F(Q_1; 1, \dots, n; \bar{Q}_2) |S_\mu(Q_1; 1, \dots, n; \bar{Q}_2) V^\mu|^2 + O\left(\frac{1}{N^2}\right) \right]. \quad (3.74)$$

As discussed in Sec. III J, the subleading color terms have a similar structure, see (3.83)–(3.85).

Similarly, the effective squared matrix elements for $e^+e^- \rightarrow q\bar{q}q\bar{q} + (n-2)g$ with an unresolved collinear pair are given by

$$\begin{aligned} |\widehat{T}_\mu V^\mu|_C^2 &= e^2 \left(\frac{g^2 N}{2} \right)^n \left(\frac{N^2 - 1}{N^2} \right) \\ &\times \sum_{P(1, \dots, n-2)} \sum_{i=0}^{n-2} \left[C_F(Q_1; 1, \dots, i; \bar{Q}_4 | Q_3; i+1, \dots, n-2; \bar{Q}_2) |\mathcal{X}_\mu^i(Q_1, \bar{Q}_2; Q_3, \bar{Q}_4) V^\mu|^2 \right. \\ &\quad \left. + C_F(Q_1; 1, \dots, i; \bar{Q}_2 | Q_3; i+1, \dots, n-2; \bar{Q}_4) |\mathcal{X}_\mu^i(Q_1, \bar{Q}_4; Q_3, \bar{Q}_2) V^\mu|^2 \right. \\ &\quad \left. + O\left(\frac{1}{N}\right) \right], \end{aligned} \quad (3.75)$$

where

$$C_F(Q_1; 1, \dots, i; \bar{Q}_4 | Q_3; i+1, \dots, n-2; \bar{Q}_2) = C_F(Q_1; 1, \dots, i; \bar{Q}_4) + C_F(Q_3; i+1, \dots, n-2; \bar{Q}_2). \quad (3.76)$$

I. The full contribution from unresolved phase space

We may now combine the results of the previous sections to calculate the full contribution from $e^+e^- \rightarrow q\bar{q} + ng$ with one unresolved parton. The effective matrix elements may be written

$$\begin{aligned} |\widehat{S}_\mu V^\mu|_S^2 + |\widehat{S}_\mu V^\mu|_C^2 &= e^2 \left(\frac{g^2 N}{2} \right)^n \left(\frac{N^2 - 1}{N} \right) \\ &\times \sum_{P(1, \dots, n)} \left[R(Q_1; 1, \dots, n; \bar{Q}_2) |S_\mu(Q_1; 1, \dots, n; \bar{Q}_2) V^\mu|^2 + O\left(\frac{1}{N^2}\right) \right], \end{aligned} \quad (3.77)$$

where $R(Q_1; 1, \dots, n; \overline{Q}_2)$ is ordered and contains all the divergences associated with the unresolved parton and is given by the sum of the ordered soft and collinear factors (3.34) and (3.73):

$$R(Q_1; 1, \dots, n; \overline{Q}_2) = S_F(Q_1; 1, \dots, n; \overline{Q}_2) + C_F(Q_1; 1, \dots, n; \overline{Q}_2). \tag{3.78}$$

Combining the results for S_F and C_F , we have

$$\begin{aligned} R(Q_1; 1, \dots, n; \overline{Q}_2) &= \left(\frac{\alpha_s N}{2\pi}\right) \frac{1}{\Gamma(1-\epsilon)} \left(\frac{4\pi\mu^2}{s_{\min}}\right)^\epsilon \frac{1}{\epsilon^2} \\ &\quad \times \left[- \left[\left(\frac{s_{Q_1 1}}{s_{\min}}\right)^\epsilon + \left(\frac{s_{12}}{s_{\min}}\right)^\epsilon + \dots + \left(\frac{s_{n\overline{Q}_2}}{s_{\min}}\right)^\epsilon \right] \right. \\ &\quad \left. + \frac{1-\epsilon}{2(3-2\epsilon)} [12(n+1) - (9n+11+2n\hat{n}_f)\epsilon + 2\epsilon^2] \frac{\Gamma^2(1-\epsilon)}{\Gamma(2-2\epsilon)} \right] \\ &= \left(\frac{\alpha_s N}{2\pi}\right) \frac{1}{\Gamma(1-\epsilon)} \left[\sum_{ij} \left\{ \frac{1}{\epsilon^2} \left(\frac{4\pi\mu^2}{s_{ij}}\right)^\epsilon - \ln^2\left(\frac{s_{ij}}{s_{\min}}\right) \right\} \right. \\ &\quad \left. + \frac{3}{2\epsilon} \left(\frac{4\pi\mu^2}{s_{\min}}\right)^\epsilon + \frac{63+67n-10n\hat{n}_f}{18} - \frac{\pi^2(n+1)}{3} \right] \\ &\quad + \frac{\alpha_s n b_0}{\epsilon} \frac{1}{\Gamma(1-\epsilon)} \left(\frac{4\pi\mu^2}{s_{\min}}\right)^\epsilon + O(\epsilon), \end{aligned} \tag{3.79}$$

where the sum is over the color charged lines, i.e., $ij = Q_1 1, 12, \dots, n\overline{Q}_2$. The one-loop QCD beta function b_0 is given by

$$b_0 = \frac{11N - 2n_f}{12\pi}. \tag{3.80}$$

It is important to note that terms of order s_{\min} have been neglected so that this equation is only valid in the small s_{\min} limit. For $n = 1$, we have checked that (3.79) reproduces the result of [38].

An analogous result holds for the four-quark process (1.5) when one of the partons is unresolved. Explicitly we find

$$\begin{aligned} \left| \widehat{T}_\mu V^\mu \right|_S^2 + \left| \widehat{T}_\mu V^\mu \right|_C^2 &= e^2 \left(\frac{g^2 N}{2}\right)^n \left(\frac{N^2-1}{N^2}\right) \\ &\quad \times \sum_{P(1, \dots, n-2)} \sum_{i=0}^{n-2} \left[R(Q_1; 1, \dots, i; \overline{Q}_4 | Q_3; i+1, \dots, n-2; \overline{Q}_2) \left| \mathcal{X}_\mu^i(Q_1, \overline{Q}_2; Q_3, \overline{Q}_4) V^\mu \right|^2 \right. \\ &\quad \left. + R(Q_1; 1, \dots, i; \overline{Q}_2 | Q_3; i+1, \dots, n-2; \overline{Q}_4) \left| \mathcal{X}_\mu^i(Q_1, \overline{Q}_4; Q_3, \overline{Q}_2) V^\mu \right|^2 \right. \\ &\quad \left. + O\left(\frac{1}{N}\right) \right], \end{aligned} \tag{3.81}$$

where, because of (3.23) and (3.56),

$$R(Q_1; 1, \dots, i; \overline{Q}_4 | Q_3; i+1, \dots, n-2; \overline{Q}_2) = R(Q_1; 1, \dots, i; \overline{Q}_4) + R(Q_3; i+1, \dots, n-2; \overline{Q}_2). \tag{3.82}$$

Once these phase space contributions are combined with the virtual corrections, and coupling constant renormalization is performed, all the poles in ϵ must cancel. On the other hand, the virtual corrections cannot give any contribution proportional to s_{\min} and $R(Q_1; 1, \dots, n; \overline{Q}_2)$ therefore contains the full dependence on the parton resolution parameter s_{\min} .

J. The terms subleading in the number of colors

As we have shown in the previous sections, the key to isolating the soft and collinear divergences lies in the soft and collinear behavior of the color ordered subamplitudes \mathcal{S}_μ and \mathcal{X}_μ . The terms subleading in the number of colors can also be expressed in terms of \mathcal{S}_μ and \mathcal{X}_μ [32]. For example, for $e^+e^- \rightarrow q\bar{q}gg$, the squared matrix elements are given by

$$\left| \widehat{S}_\mu V^\mu \right|^2 = e^2 \left(\frac{g^2 N}{2}\right)^2 \left(\frac{N^2-1}{N}\right) \left[\sum_{P(1,2)} \left| \mathcal{S}_\mu(Q_1; 1, 2; \overline{Q}_2) V^\mu \right|^2 - \frac{1}{N^2} \left| \mathcal{S}_\mu(Q_1; \tilde{1}, \tilde{2}; \overline{Q}_2) V^\mu \right|^2 \right], \tag{3.83}$$

where the second term has been symmetrized with respect to the two gluons:

$$\mathcal{S}_\mu(Q_1; \tilde{1}, \tilde{2}; \overline{Q}_2) = \mathcal{S}_\mu(Q_1; 1, 2; \overline{Q}_2) + \mathcal{S}_\mu(Q_1; 2, 1; \overline{Q}_2). \quad (3.84)$$

In this subamplitude, there is no contribution from the triple gluon vertex and the gluons behave as photons [32]. There is effectively only one color line connecting the quark and antiquark. The soft and collinear behavior is then straightforward,

$$\begin{aligned} \left| \mathcal{S}_\mu(Q_1; \tilde{1}, \tilde{2}; \overline{Q}_2) V^\mu \right|^2 &\rightarrow (S_F(Q_1; \overline{Q}_2) + C_F(Q_1; \overline{Q}_2)) \left| \mathcal{S}_\mu(Q_1; 1; \overline{Q}_2) V^\mu \right|^2 \\ &\rightarrow R(Q_1; \overline{Q}_2) \left| \mathcal{S}_\mu(Q_1; 1; \overline{Q}_2) V^\mu \right|^2. \end{aligned} \quad (3.85)$$

The virtual diagrams follow a similar structure and the full next-to-leading order matrix elements for $e^+e^- \rightarrow q\bar{q}gg$ are given by (A41). In general, however, the subleading terms depend on the number of partons and no general form is available. Nevertheless, these terms do not present any significant difficulties and the dynamical R factors associated with them are given by the leading- N R factors for processes containing fewer partons.

IV. VIRTUAL CONTRIBUTIONS

At leading order in the number of colors, the complete next-to-leading-order cross section is obtained by adding the one-loop virtual contribution to the single parton unresolved cross section of the previous section. In this section, we will discuss the process $e^+e^- \rightarrow q\bar{q} + ng$ in detail, while we will only make a few remarks on the four-quark process.

The virtual graphs for $e^+e^- \rightarrow q\bar{q} + ng$ are formed by attaching an internal gluon (with color x) in all possible permutations to the tree level amplitude (3.9) which generates color structures of the form, $(T^{a_1} \dots T^x \dots T^{a_m} \dots T^x \dots T^{a_n})_{c_1 c_2}$. When the color matrices T^x are adjacent (which corresponds to emission and absorption of the virtual gluon on the same color charged line), this gives an additional factor of $(N^2 - 1)/2N$ relative to tree level. On the other hand, if color matrices associated with the hard partons are inserted between the internal color matrices, only terms subleading in the number of colors are generated. Keeping only the leading N contribution yields the next-to-leading-order current $\widehat{\mathcal{S}}_\mu^{(1)}$ which may be decomposed according to the color structure as in (3.9):

$$\widehat{\mathcal{S}}_\mu^{(1)}(Q_1; 1, \dots, n; \overline{Q}_2) = ieg^n \left(\frac{g^2 N}{2} \right) \sum_{P(1, \dots, n)} \left[(T^{a_1} \dots T^{a_n})_{c_1 c_2} \mathcal{S}_\mu^{(1)}(Q_1; 1, \dots, n; \overline{Q}_2) + O\left(\frac{1}{N^2}\right) \right]. \quad (4.1)$$

The next-to-leading-order ordered subcurrent $\mathcal{S}_\mu^{(1)}$ may be written as a part proportional to the lowest-order current \mathcal{S}_μ containing all of the virtual soft and collinear singularities, and a part that is finite as $\epsilon \rightarrow 0$ and can have a different structure from tree level, $\overline{\mathcal{S}}_\mu^{(1)}$:

$$\mathcal{S}_\mu^{(1)}(Q_1; 1, \dots, n; \overline{Q}_2) = f_V \mathcal{S}_\mu(Q_1; 1, \dots, n; \overline{Q}_2) + \overline{\mathcal{S}}_\mu^{(1)}(Q_1; 1, \dots, n; \overline{Q}_2). \quad (4.2)$$

It should be noted that there is always some arbitrariness between the assignment of the finite pieces between the two terms.

By multiplying the one-loop contribution by the lowest-order matrix element, we obtain the virtual next-to-leading-order effective matrix elements at leading order in the number of colors:

$$\begin{aligned} \left| \widehat{\mathcal{S}}_\mu V^\mu \right|_V^2 &= e^2 \left(\frac{g^2 N}{2} \right)^n \left(\frac{N^2 - 1}{N} \right) \\ &\times \sum_{P(1, \dots, n)} \left[V(Q_1; 1, \dots, n; \overline{Q}_2) \left| \mathcal{S}_\mu(Q_1; 1, \dots, n; \overline{Q}_2) V^\mu \right|^2 + \mathcal{F}(Q_1; 1, \dots, n; \overline{Q}_2) + O\left(\frac{1}{N^2}\right) \right], \end{aligned} \quad (4.3)$$

where

$$\mathcal{F}(Q_1; 1, \dots, n; \overline{Q}_2) = \left(\frac{g^2 N}{2} \right) 2 \operatorname{Re} \left\{ \left(\mathcal{S}_\mu(Q_1; 1, \dots, n; \overline{Q}_2) V^\mu \right) \left(\overline{\mathcal{S}}_\nu^{(1)}(Q_1; 1, \dots, n; \overline{Q}_2) V^\nu \right)^\dagger \right\}, \quad (4.4)$$

is finite. The ordered virtual factor, V , has the structure

$$\begin{aligned} V(Q_1; 1, \dots, n; \overline{Q}_2) &= \left(\frac{g^2 N}{2} \right) 2 \operatorname{Re}(f_V) \\ &= \left(\frac{\alpha_s N}{2\pi} \right) \frac{\Gamma(1 + \epsilon) \Gamma^2(1 - \epsilon)}{\Gamma(1 - 2\epsilon)} \left[V_{Q_1 1} + V_{1 2} + \dots + V_{n \overline{Q}_2} \right], \end{aligned} \quad (4.5)$$

where V_{ab} represents the divergent virtual contribution which arises when the internal gluon is attached to the color-charged line joining hard partons a and b . V_{ab} will, of course, contain precisely the right soft and collinear singularities to cancel the contributions from the single-parton unresolved cross section.

Let us first consider the soft contributions and return to our QED example of n photons attached to a charged fermion line (Sec. III C). The one-loop corrections to this process are obtained by the emission and subsequent re-absorption of a photon from the charged fermion line. In the soft limit, off-shell photon emission is characterized by the gauge-invariant factor

$$E_\mu(Q, P; \ell) = \left(\frac{2Q_\mu + \ell_\mu}{\ell^2 + 2Q \cdot \ell} - \frac{2P_\mu + \ell_\mu}{\ell^2 + 2P \cdot \ell} \right), \quad (4.6)$$

where ℓ_μ is the momentum of the soft off-shell photon [34]. Note that in the on-shell limit, this reduces to the eikonal factor of (3.17). As in the on-shell photon case, only virtual soft photon radiation from external lines contributes to the pole in $1/\epsilon^2$.

Since the emission of a soft photon cannot change the correlation between the hard particles, the soft virtual contribution is proportional to tree level:

$$\mathcal{M}_{\text{soft}}^{(1)}(Q; 1, \dots, n; P) = f_{\text{QED}}^{\text{soft}} \mathcal{M}(Q; 1, \dots, n; P), \quad (4.7)$$

where

$$f_{\text{QED}}^{\text{soft}} = \frac{e^2}{2} \int \frac{d^d \ell}{(2\pi)^d} E_\mu(Q, P; \ell) P^{\mu\nu} E_\nu(Q, P; -\ell). \quad (4.8)$$

The factor $1/2$ is due to Bose statistics of the emitted/absorbed photon. In principle there is some dependence on the loop momenta remaining in \mathcal{M} ; however, this disappears in the soft photon limit. In the light-

cone gauge, the internal photon propagator $P^{\mu\nu}$ is given by

$$P^{\mu\nu} = \frac{-i}{\ell^2} \left(g^{\mu\nu} - \frac{(b^\mu \ell^\nu + \ell^\mu b^\nu)}{b \cdot \ell} \right), \quad (4.9)$$

where b_μ is a lightlike auxiliary vector. Since E_μ is gauge invariant, the gauge-dependent terms cancel trivially and we only need to keep the terms proportional to $g^{\mu\nu}$.

Only the real part of $f_{\text{QED}}^{\text{soft}}$ contributes and we define the soft virtual contributions V_{QP}^{soft} to be only the terms associated with the pole of order $1/\epsilon^2$. To be explicit,

$$\begin{aligned} \text{Re}(f_{\text{QED}}^{\text{soft}}) &= \left(\frac{\alpha}{2\pi} \right) \frac{\Gamma(1+\epsilon)\Gamma^2(1-\epsilon)}{\Gamma(1-2\epsilon)} \\ &\times \left[V_{QP}^{\text{soft}} - \left(\frac{4\pi\mu^2}{s_{QP}} \right)^\epsilon \frac{1}{2\epsilon(1-2\epsilon)} \right], \end{aligned} \quad (4.10)$$

where the soft factor depends only on the invariant mass of the electron-positron pair, s_{QP} and the explicit $1/\epsilon$ terms within the square brackets by definition contribute to the collinear virtual part and have to be combined with the other virtual collinear contributions. The soft factor is given by

$$\begin{aligned} V_{QP}^{\text{soft}} &= -\frac{\text{Re}(-1)^\epsilon}{\epsilon^2} \left(\frac{4\pi\mu^2}{s_{QP}} \right)^\epsilon \\ &= -\frac{1}{\epsilon^2} \left(\frac{4\pi\mu^2}{s_{QP}} \right)^\epsilon + \frac{\pi^2}{2} + O(\epsilon). \end{aligned} \quad (4.11)$$

As in the on-shell case, QCD has a completely analogous behavior to QED, where now each color-charged line (containing either gluons or quarks) yields precisely the same virtual soft contribution:

$$V_{q\bar{q}}^{\text{soft}} = V_{g\bar{g}}^{\text{soft}} = V_{g\bar{q}}^{\text{soft}} = V_{g\bar{g}}^{\text{soft}}. \quad (4.12)$$

The ordered virtual factor (4.5) is therefore given by

$$\begin{aligned} V(Q_1; 1, \dots, n; \bar{Q}_2) &= \left(\frac{\alpha_s N}{2\pi} \right) \frac{\Gamma(1+\epsilon)\Gamma^2(1-\epsilon)}{\Gamma(1-2\epsilon)} \left(\sum_{ij} V_{ij}^{\text{soft}} + V^{\text{col}} \right) \\ &= \left(\frac{\alpha_s N}{2\pi} \right) \frac{\Gamma(1+\epsilon)\Gamma^2(1-\epsilon)}{\Gamma(1-2\epsilon)} \left[-\frac{1}{\epsilon^2} \sum_{ij} \left(\frac{4\pi\mu^2}{s_{ij}} \right)^\epsilon + \frac{\pi^2(n+1)}{2} + V^{\text{col}} \right], \end{aligned} \quad (4.13)$$

where the sum is over the $n+1$ color-connected pairs, $Q_1 1, 2, \dots, n, \bar{Q}_2$. The remaining virtual collinear divergences V^{col} are of order $1/\epsilon$ and must contain precisely the right single poles in ϵ to cancel those from the unresolved portion of phase space.

At next-to-leading order, the unrenormalized full squared matrix elements for $e^+e^- \rightarrow q\bar{q} + ng$ are obtained by summing the real soft and collinear parts (3.79) with the virtual contribution (4.3):

$$\begin{aligned} |\widehat{\mathcal{S}}_\mu V^\mu|_F^2 &= |\widehat{\mathcal{S}}_\mu V^\mu|_S^2 + |\widehat{\mathcal{S}}_\mu V^\mu|_C^2 + |\widehat{\mathcal{S}}_\mu V^\mu|_V^2 \\ &= e^2 \left(\frac{g^2 N}{2} \right)^n \left(\frac{N^2 - 1}{N} \right) \\ &\times \sum_{P(1, \dots, n)} \left[\mathcal{K}(Q_1; 1, \dots, n; \bar{Q}_2) \left| \mathcal{S}_\mu(Q_1; 1, \dots, n; \bar{Q}_2) V^\mu \right|^2 + \mathcal{F}(Q_1; 1, \dots, n; \bar{Q}_2) + O\left(\frac{1}{N^2}\right) \right], \end{aligned} \quad (4.14)$$

which has the structure of tree level, (3.12), where each subamplitude is now multiplied by a next-to-leading-order ordered dynamical \mathcal{K} factor and added to a finite non-tree-level ordered structure \mathcal{F} determined by the one-loop graphs. Using the relationship

$$\frac{\Gamma(1+\epsilon)\Gamma^2(1-\epsilon)}{\Gamma(1-2\epsilon)} = \frac{1}{\Gamma(1-\epsilon)} + O(\epsilon^3), \quad (4.15)$$

we find the unrenormalized next-to-leading-order dynamical \mathcal{K} factor to be given by

$$\begin{aligned} \mathcal{K}(Q_1; 1, \dots, n; \overline{Q}_2) &= R(Q_1; 1, \dots, n; \overline{Q}_2) + V(Q_1; 1, \dots, n; \overline{Q}_2) \\ &= \left(\frac{\alpha_s N}{2\pi} \right) \frac{1}{\Gamma(1-\epsilon)} \\ &\quad \times \left[-\sum_{ij} \ln^2 \left(\frac{s_{ij}}{s_{\min}} \right) + \frac{\pi^2(n+1)}{6} + V^{\text{col}} + \frac{3}{2\epsilon} \left(\frac{4\pi\mu^2}{s_{\min}} \right)^\epsilon + \frac{63+67n-10n\hat{n}_f}{18} \right] \\ &\quad + \frac{\alpha_s b_0 n}{\epsilon} \frac{1}{\Gamma(1-\epsilon)} \left(\frac{4\pi\mu^2}{s_{\min}} \right)^\epsilon + O(\epsilon) + O(s_{\min}). \end{aligned} \quad (4.16)$$

Although the virtual collinear factors are undetermined, they must satisfy the relationship

$$V^{\text{col}} = -\frac{3}{2\epsilon} + \text{finite pieces}, \quad (4.17)$$

which is necessary to ensure that all the collinear poles cancel. The finite pieces may be either single logarithms or constants. Note that the divergent contribution is independent of the number of gluons involved in the process. Furthermore, the $-3/2\epsilon$ pole is associated with the fact that we take the fermions massless and is present in both QED and QCD. It is worth noting that in QED, the \mathcal{K} factor is simply given by (4.16) with $n=0$ and the replacement $\alpha_s N/2 \rightarrow \alpha$.

By calculating the virtual corrections for $e^+e^- \rightarrow q\bar{q}$ and $e^+e^- \rightarrow q\bar{q} + g$ we can make a ‘‘natural’’ choice of the finite pieces in (4.17). First of all we rewrite the collinear factor to accommodate the ordered gluon structure of the subamplitudes:

$$V^{\text{col}} = \sum_{ij} V_{ij}^{\text{col}}(s_{ij}) + C^{\text{col}}, \quad (4.18)$$

where C^{col} is an arbitrary constant and the sum is over the ordered pairs.

Explicit calculation of the virtual corrections to $e^+e^- \rightarrow q\bar{q}$ using the methods of [39] yields

$$V(Q_1; \overline{Q}_2) = \left(\frac{\alpha_s N}{2\pi} \right) \frac{\Gamma(1+\epsilon)\Gamma^2(1-\epsilon)}{\Gamma(1-2\epsilon)} \left[-\frac{1}{\epsilon^2} \left(\frac{4\pi\mu^2}{s_{Q_1\overline{Q}_2}} \right)^\epsilon + \frac{\pi^2}{2} - \frac{3}{2\epsilon} \left(\frac{4\pi\mu^2}{s_{Q_1\overline{Q}_2}} \right)^\epsilon - 4 \right] + O(\epsilon), \quad (4.19)$$

$$\mathcal{F}(Q_1; \overline{Q}_2) = 0,$$

with the ‘‘natural’’ choice of the finite contribution equal to zero. Comparing this expression with (4.13) leads us to make the following choice for V^{col} :

$$V_{q\bar{q}}^{\text{col}}(s_{Q_1\overline{Q}_2}) = -\frac{3}{2\epsilon} \left(\frac{4\pi\mu^2}{s_{Q_1\overline{Q}_2}} \right)^\epsilon - 4, \quad C^{\text{col}} = 0, \quad (4.20)$$

so that

$$V(Q_1; \overline{Q}_2) = \left(\frac{\alpha_s N}{2\pi} \right) \frac{\Gamma(1+\epsilon)\Gamma^2(1-\epsilon)}{\Gamma(1-2\epsilon)} \left(V_{q\bar{q}}^{\text{soft}}(s_{Q_1\overline{Q}_2}) + V_{q\bar{q}}^{\text{col}}(s_{Q_1\overline{Q}_2}) \right). \quad (4.21)$$

Combining this with the resolved phase space factor $R(Q_1; \overline{Q}_2)$ [(3.79) with $n=0$] yields the two-quark \mathcal{K} factor

$$\begin{aligned} \mathcal{K}(Q_1; \overline{Q}_2) &= R(Q_1; \overline{Q}_2) + V(Q_1; \overline{Q}_2) \\ &= \left(\frac{\alpha_s N}{2\pi} \right) \left[-\ln^2 \left(\frac{s_{Q_1\overline{Q}_2}}{s_{\min}} \right) + \frac{\pi^2}{6} + \frac{3}{2} \ln \left(\frac{s_{Q_1\overline{Q}_2}}{s_{\min}} \right) - \frac{1}{2} \right] + O(\epsilon) + O(s_{\min}). \end{aligned} \quad (4.22)$$

Similarly, calculation of the virtual corrections to $e^+e^- \rightarrow q\bar{q} + g$ at leading order in the number of colors, leads to

the expression

$$V(Q_1; 1; \bar{Q}_2) = \left(\frac{\alpha_s N}{2\pi} \right) \frac{\Gamma(1+\epsilon)\Gamma^2(1-\epsilon)}{\Gamma(1-2\epsilon)} \times \left[-\frac{1}{\epsilon^2} \left(\frac{4\pi\mu^2}{s_{Q_1 1}} \right)^\epsilon - \frac{1}{\epsilon^2} \left(\frac{4\pi\mu^2}{s_1 \bar{Q}_2} \right)^\epsilon + \pi^2 - \frac{3}{4\epsilon} \left(\frac{4\pi\mu^2}{s_{Q_1 1}} \right)^\epsilon - \frac{3}{4\epsilon} \left(\frac{4\pi\mu^2}{s_1 \bar{Q}_2} \right)^\epsilon - 4 \right] + O(\epsilon). \quad (4.23)$$

An expression for the finite non-tree-level terms $\mathcal{F}(Q_1; 1; \bar{Q}_2)$ is given in the Appendix. Again, comparing with (4.13) leads us to the “natural” choice

$$V_{qg}^{\text{col}}(s) = V_{g\bar{q}}^{\text{col}}(s) = \frac{1}{2} V_{q\bar{q}}^{\text{col}}(s) = -\frac{3}{4\epsilon} \left(\frac{4\pi\mu^2}{s} \right)^\epsilon - 2, \quad C^{\text{col}} = 0, \quad (4.24)$$

such that

$$V(Q_1; 1; \bar{Q}_2) = \left(\frac{\alpha_s N}{2\pi} \right) \frac{\Gamma(1+\epsilon)\Gamma^2(1-\epsilon)}{\Gamma(1-2\epsilon)} \left(V_{qg}^{\text{soft}}(s_{Q_1 1}) + V_{g\bar{q}}^{\text{col}}(s_{Q_1 1}) + V_{g\bar{q}}^{\text{soft}}(s_1 \bar{Q}_2) + V_{g\bar{q}}^{\text{col}}(s_1 \bar{Q}_2) \right). \quad (4.25)$$

Adding the resolved phase space factor $R(Q_1; 1; \bar{Q}_2)$ [(3.79) with $n = 1$] gives the dynamical \mathcal{K} factor for $e^+e^- \rightarrow q\bar{q}+g$:

$$\begin{aligned} \mathcal{K}(Q_1; 1; \bar{Q}_2) &= R(Q_1; 1; \bar{Q}_2) + V(Q_1; 1; \bar{Q}_2) \\ &= \left(\frac{\alpha_s N}{2\pi} \right) \left[-\ln^2 \left(\frac{s_{Q_1 1}}{s_{\text{min}}} \right) - \ln^2 \left(\frac{s_1 \bar{Q}_2}{s_{\text{min}}} \right) + \frac{\pi^2}{3} + \frac{3}{4} \ln \left(\frac{s_{Q_1 1}}{s_{\text{min}}} \right) + \frac{3}{4} \ln \left(\frac{s_1 \bar{Q}_2}{s_{\text{min}}} \right) + \frac{29}{9} - \frac{5n_f}{9N} \right] \\ &\quad + \frac{\alpha_s b_0}{\epsilon} \frac{1}{\Gamma(1-\epsilon)} \left(\frac{4\pi\mu^2}{s_{\text{min}}} \right)^\epsilon + O(\epsilon) + O(s_{\text{min}}). \end{aligned} \quad (4.26)$$

We see that the only remaining poles in (4.26) are ultraviolet in origin, and are proportional to the one-loop QCD beta function b_0 , and are therefore associated with coupling constant renormalization. In the modified minimal subtraction ($\overline{\text{MS}}$) scheme [40], the coupling constant is redefined in terms of the coupling constant evaluated at the renormalization scale μ by

$$\alpha_s = \alpha_s(\mu^2) \left(1 - \frac{\alpha_s(\mu^2) b_0}{\bar{\epsilon}} \right), \quad (4.27)$$

where

$$\frac{1}{\bar{\epsilon}} = \frac{1}{\epsilon} \frac{(4\pi)^\epsilon}{\Gamma(1-\epsilon)} = \frac{1}{\epsilon} + \ln(4\pi) - \gamma_E + O(\epsilon), \quad (4.28)$$

and γ_E is the Euler constant. At next-to-leading order, the strong coupling constant at scale μ is defined relative to the fundamental QCD scale $\Lambda_{\overline{\text{MS}}}$ to be

$$\alpha_s(\mu^2) = \frac{1}{b_0 \ln \left(\mu^2 / \Lambda_{\overline{\text{MS}}}^2 \right)} \left(1 - \frac{b_1 \ln \left[\ln \left(\mu^2 / \Lambda_{\overline{\text{MS}}}^2 \right) \right]}{b_0^2 \ln \left(\mu^2 / \Lambda_{\overline{\text{MS}}}^2 \right)} \right), \quad (4.29)$$

with

$$b_1 = \frac{34N^2 - 13Nn_f + 3n_f/N}{48\pi^2}. \quad (4.30)$$

As discussed in Sec. III J, the subleading color terms have a similar structure; see (3.83)–(3.85) and (A39)–(A41).

It is now straightforward to generalize the \mathcal{K} factor of (4.26) to include more gluons. By inspection of (4.16), we see that V_{qg}^{col} cannot be singular as $\epsilon \rightarrow 0$. Therefore, by choosing $C^{\text{col}} = 0$ and $V_{qg}^{\text{col}}(s) = 0$ we can uniquely define V^{col} . Any additional finite terms are thereby assigned to \mathcal{F} , and the dynamical \mathcal{K} factor (4.16) is fully defined. The only remaining poles are the ultraviolet poles proportional to b_0 . Since the lowest-order squared matrix element (3.12) is proportional to α_s^n , the coupling constant redefinition (4.27) precisely cancels the ultraviolet poles in (4.16). The finite, renormalized \mathcal{K} factor for any number of gluons is, thus,

$$\begin{aligned}
\mathcal{K}(Q_1; 1, \dots, n; \bar{Q}_2) &= \left(\frac{\alpha_s(\mu^2)N}{2\pi} \right) \left[\sum_{ij} \left\{ -\ln^2 \left(\frac{s_{ij}}{s_{\min}} \right) \right\} + \frac{\pi^2(n+1)}{6} + \frac{3}{4} \ln \left(\frac{s_{Q_1 1}}{s_{\min}} \right) \right. \\
&\quad \left. + \frac{3}{4} \ln \left(\frac{s_{n\bar{Q}_2}}{s_{\min}} \right) + \frac{67n-9-10n\hat{n}_f}{18} \right] \\
&\quad + \alpha_s(\mu^2)b_0n \ln \left(\frac{\mu^2}{s_{\min}} \right) + O(\epsilon) + O(s_{\min}). \tag{4.31}
\end{aligned}$$

As might be expected from our earlier discussion of the soft and collinear limits of the real graphs, an analogous result holds for the four quark process (1.5). After coupling constant renormalization

$$\begin{aligned}
|\hat{T}_\mu V^\mu|_F^2 &= e^2 \left(\frac{g^2(\mu)N}{2} \right)^n \left(\frac{N^2-1}{N^2} \right) \\
&\times \sum_{P(1, \dots, n-2)} \sum_{i=0}^{n-2} \left[\mathcal{K}(Q_1; 1, \dots, i; \bar{Q}_4|Q_3; i+1, \dots, n-2; \bar{Q}_2) \left| \mathcal{X}_\mu^i(Q_1, \bar{Q}_2; Q_3, \bar{Q}_4)V^\mu \right|^2 \right. \\
&\quad + \mathcal{F}(Q_1; 1, \dots, i; \bar{Q}_4|Q_3; i+1, \dots, n-2; \bar{Q}_2) \\
&\quad + \mathcal{K}(Q_1; 1, \dots, i; \bar{Q}_2|Q_3; i+1, \dots, n-2; \bar{Q}_4) \left| \mathcal{X}_\mu^i(Q_1, \bar{Q}_4; Q_3, \bar{Q}_2)V^\mu \right|^2 \\
&\quad \left. + \mathcal{F}(Q_1; 1, \dots, i; \bar{Q}_2|Q_3; i+1, \dots, n-2; \bar{Q}_4) + O\left(\frac{1}{N}\right) \right], \tag{4.32}
\end{aligned}$$

where the dynamical \mathcal{K} -factor is now given by a sum of two two-quark \mathcal{K} factors:

$$\mathcal{K}(Q_1; 1, \dots, i; \bar{Q}_4|Q_3; i+1, \dots, n-2; \bar{Q}_2) = \mathcal{K}(Q_1; 1, \dots, i; \bar{Q}_4) + \mathcal{K}(Q_3; i+1, \dots, n-2; \bar{Q}_2). \tag{4.33}$$

It is important to note that the coefficient of $b_0/\bar{\epsilon}$ in $R(Q_1; 1, \dots, i; \bar{Q}_4|Q_3; i+1, \dots, n-2; \bar{Q}_2)$ is equal to the number of final-state gluons which is now $(n-2)$. The coupling-constant renormalization, however, generates a counterterm of $-nb_0/\bar{\epsilon}$, making \mathcal{K} apparently divergent. This is not, of course, the case since, unlike the two-quark virtual corrections, the four-quark $V(Q_1; 1, \dots, i; \bar{Q}_4|Q_3; i+1, \dots, n-2; \bar{Q}_2)$ contains additional ultraviolet poles, proportional to $2b_0/\bar{\epsilon}$, which render the cross section finite. Any additional finite terms associated with the virtual ultraviolet poles are reassigned to \mathcal{F} .

V. NUMERICAL RESULTS

With the methods described in the previous sections, and using the matrix elements given in the Appendix, we can construct a Monte Carlo program which generates resolved n -parton and $(n+1)$ -parton events with their corresponding (finite, but not necessarily positive) weights.

By themselves these resolved parton cross sections have no physical meaning and will depend strongly on our theoretical parton resolution parameter, s_{\min} . However for physical next-to-leading-order n -jet cross sections, both the n -parton and the $(n+1)$ -parton cross sections contribute and are combined according to the jet cluster algorithm, rendering the resulting n -jet cross section independent of s_{\min} .

The cancellation of the s_{\min} dependence is performed numerically by the Monte Carlo program. Although the logarithmic s_{\min} dependence of the n -parton cross sec-

tion is explicitly shown in \mathcal{K} , the counterterms from the $(n+1)$ -parton contribution are determined by the Monte Carlo evaluation. For this reason we do not want to take s_{\min} too small so that we can avoid large numerical cancellations. On the other hand choosing s_{\min} too large introduces a systematic error due to the fact that we use the collinear and soft approximations to obtain factorization and are forced to neglect term of order s_{\min} .

The Monte Carlo program written according to the above philosophy allows one to keep all the correlations of the event and allows for an easy numerical implementation of the jet algorithm, detector acceptance and any additional cuts. In the next two subsections we will discuss two explicit examples of next-to-leading-order jet production, $e^+e^- \rightarrow 2$ jets and $e^+e^- \rightarrow 3$ jets. For the purposes of illustration, the beam energy is always chosen to be the Z -boson mass, M_Z , and no QED initial-state radiation is included. Furthermore, the factorization scale μ at which the strong coupling constant $\alpha_s(\mu^2)$ is evaluated is chosen to be M_Z unless otherwise stated.

In most of the explicit examples we will choose a limited number of events generated in the Monte Carlo simulation in order to show the interplay between the statistical and systematic errors. For a more phenomenologically orientated study one can easily increase the number of events, thereby reducing the error in the Monte Carlo simulation to the desired value.

To indicate the number of events used to estimate the n -jet cross section, we will use the notation $x(y_1 + y_2)$ which means xy_1 n -parton events and xy_2 $(n+1)$ -parton events are evaluated. In other words, the n -jet cross section is evaluated x times with $y_1 + y_2$ terms. The cross section is taken to be the average of the x results,

while the error is estimated by their standard deviation. For differential cross sections, the estimate and error are given on a bin by bin basis.

In order to illustrate the sensitivity of next-to-leading-order jet cross sections on the jet algorithm (and the adaptability of the Monte Carlo approach), we will use several, more or less standardized, jet definitions which are the E , $E0$, and P schemes. For each scheme, if the smallest invariant mass of any pair of all possible final state momenta is smaller than an experimental value s_{cut} , the corresponding two momenta are replaced by a recombined momentum, thus reducing the number of momenta in the final state by 1. This procedure is repeated until all invariant masses are larger than s_{cut} , the remaining momenta are the jet axis momenta. The difference between the schemes is in how the parton (or hadron) momenta are recombined to give a composite momentum. The recombined momentum is given by

$$P_{\text{rec}}^\mu = (E_{\text{rec}}, \mathbf{P}_{\text{rec}}), \quad (5.1)$$

where,

$$E_{\text{rec}} = \alpha (E_1 + E_2), \quad (5.2)$$

$$\mathbf{P}_{\text{rec}} = \beta (\mathbf{P}_1 + \mathbf{P}_2),$$

and where α and β are scheme dependent and are given in Table I. As shown in Table I, the E scheme conserves energy-momentum, while the $E0$ scheme conserves only energy and the P scheme conserves only momentum. On the other hand, only in the E scheme is the recombined momentum not massless.

A. Monte Carlo results for $e^+e^- \rightarrow 2$ jets

We will now discuss the results from the Monte Carlo approach to the two-jet production at next-to-leading order in α_s and keeping all orders in the number of colors. The order- α_s two-jet cross section receives contributions from two sources. One is the resolved two-parton cross section, while the other contribution stems from the lowest-order resolved three-parton cross section where two of the partons are clustered together to form the jet axis according to the chosen jet algorithm.

Because of the low parton multiplicity in the final state, some analytic results can be obtained for the two-jet cross section as a function of the jet defining cut s_{cut} . This gives us the opportunity to compare the performance of the Monte Carlo program with the analytic result.

The analytic two-jet cross section at order α_s for any of the jet schemes, is given by

$$\sigma_{2 \text{ jet}}(y_{\text{cut}}) = \sigma_0 \left\{ 1 + \frac{3}{8\pi} \alpha_s(\mu^2) \frac{N^2 - 1}{N} \left[\theta\left(y_{\text{cut}} - \frac{1}{3}\right) + \theta\left(\frac{1}{3} - y_{\text{cut}}\right) I(y_{\text{cut}}) \right] \right\}. \quad (5.3)$$

If $y_{\text{cut}} = s_{\text{cut}}/Q^2 \geq \frac{1}{3}$, it is no longer possible to generate three-parton events due to momentum conservation and therefore the two-jet cross section is equal to the total hadronic order- α_s cross section. The Born cross section, σ_0 , is the lowest-order contribution to the hadronic cross section. The function $I(y_{\text{cut}})$ is given by

$$I(y_{\text{cut}}) = \frac{4}{3} \left[\frac{\pi^2}{6} - \frac{1}{2} - 2 \text{Li}_2\left(\frac{y_{\text{cut}}}{1 - y_{\text{cut}}}\right) - \ln^2\left(\frac{y_{\text{cut}}}{1 - y_{\text{cut}}}\right) - \frac{3}{2}(1 - 2y_{\text{cut}}) \ln\left(\frac{y_{\text{cut}}}{1 - 2y_{\text{cut}}}\right) + 3y_{\text{cut}} + \frac{9}{4}y_{\text{cut}}^2 \right], \quad (5.4)$$

where the dilogarithm function Li_2 is defined by

$$\text{Li}_2(x) = - \int_0^x \frac{\ln(1-z)}{z} dz. \quad (5.5)$$

Note that in taking the limit $y_{\text{cut}} \rightarrow y_{\text{min}} = s_{\text{min}}/Q^2$, and thus ignoring terms of order y_{min} , we recover the resolved two-parton cross section (4.22). Furthermore, $I(\frac{1}{3}) = 1$, so that the two-jet cross section is continuous over the $y_{\text{cut}} = \frac{1}{3}$ boundary. The total two-jet cross section is independent of the chosen jet scheme at $O(\alpha_s)$. However, specific distributions may exhibit scheme dependence.

As discussed earlier, s_{min} is an arbitrary parameter and any physically measurable quantity should not depend on it. We therefore show the s_{min} dependence of the Monte Carlo estimate of the two-jet cross section in Figs. 1(a)–1(c) where the ratio $K_2 = \sigma_{2 \text{ jet}}(y_{\text{cut}})/\sigma_0$ is shown as a function of $y_{\text{min}}/y_{\text{cut}}$ for different values of the experimental cut y_{cut} . In order to show the interplay between the statistical and systematic errors clearly, the cross section was evaluated with a limited number of

events, $10 \times (10000 + 10000)$. For comparison, the analytic result (5.3) is shown as a solid line while the Born cross section is shown dotted.

In the Monte Carlo simulation we cannot take the limit $y_{\text{min}}/y_{\text{cut}} \rightarrow 0$ due to the logarithmic y_{min} cancellation. In fact, from the point of view of the statistical errors in the Monte Carlo simulation we want to choose $y_{\text{min}}/y_{\text{cut}}$ as large as possible in order to avoid large cancellations between the two and three parton contributions. However choosing this ratio too large would induce a system-

TABLE I. Values for the scheme-dependent recombination factors of (5.2) and $\Delta = (E_1 + E_2)/|\mathbf{P}_1 + \mathbf{P}_2|$.

	Energy rescaling factor α	Momentum rescaling factor β
E scheme	1	1
$E0$ scheme	1	Δ
P scheme	Δ^{-1}	1

atic error due to terms of $O(y_{\min})$ which are not included in the Monte Carlo error estimate. This is clearly seen in Figs. 1(a)–1(c), where at relatively large y_{\min} the statistical error is very small but the deviation from the analytic result is large. So from the point of view of the systematic errors we have to choose y_{\min}/y_{cut} as small as possible.

The compromise between these two conflicting requirements is that we must choose y_{\min}/y_{cut} such that the statistical Monte Carlo error starts to dominate over the systematic error. This implies that the right choice of y_{\min}/y_{cut} depends on the number of events used in the evaluation of the parton cross sections. Increasing the number of events will decrease the statistical error while leaving the systematic error unchanged. To avoid becoming sensitive to the systematic error, one should therefore choose a smaller value of y_{\min}/y_{cut} . To demonstrate this procedure, we choose $y_{\min}/y_{\text{cut}} = 0.10$. For $y_{\text{cut}} = 0.03$ [Fig. 1(b)] and $y_{\text{cut}} = 0.01$ [Fig. 1(c)] we are clearly within the statistically dominated region. On the other hand, for $y_{\text{cut}} = 0.10$ [Fig. 1(a)] we are on the borderline and for $y_{\text{cut}} > 0.10$ the Monte Carlo simulation will make a

systematic error. This is shown in Fig. 1(d) where we plot the two-jet cross section as a function of y_{cut} with $y_{\min} = y_{\text{cut}}/10$ for $10 \times (10,000 + 10,000)$ events. Even with this limited number of events, the Monte Carlo errors for a practical application are quite acceptable. The solid line is the analytic result (5.3). As can be seen for $y_{\text{cut}} < 0.10$, within statistical errors, the Monte Carlo estimate for the two-jet cross section agrees well with the analytic result. However for $y_{\text{cut}} > 0.10$ a clear deviation from the analytic answer develops due to the systematic error generated by our approximations. Of course, choosing the ratio y_{\min}/y_{cut} smaller in this region, e.g., $y_{\min}/y_{\text{cut}} = 0.01$, removes the systematic error.

Since the integration over the jet momenta is done by the Monte Carlo simulation, we can examine the next-to-leading-order corrections to any variable in two-jet events. To illustrate this flexibility, we show an assortment of differential cross sections in Fig. 2, where we have chosen $y_{\text{cut}} = 0.03$, $y_{\min} = y_{\text{cut}}/10$ and $10 \times (10,000 + 10,000)$ events. The leading-order results are given by the solid lined histogram, while the next-to-leading result is shown as data points with statistical errors.

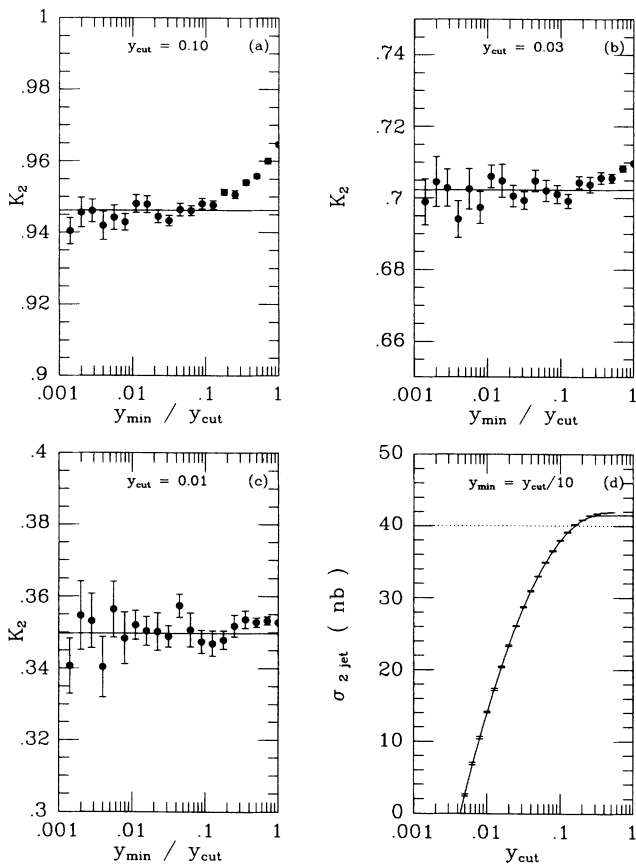


FIG. 1. The next-to-leading-order K factor, $K_2 = \sigma^{\text{NLO}}/\sigma^{\text{LO}}$, for two-jet production as a function of y_{\min}/y_{cut} for (a) $y_{\text{cut}} = 0.10$, (b) $y_{\text{cut}} = 0.03$ and (c) $y_{\text{cut}} = 0.01$ with statistical errors. The analytic results of (5.3) are shown as solid lines. Part (d) shows the y_{cut} dependence of the next-to-leading-order two-jet cross section for $y_{\min}/y_{\text{cut}} = 0.1$ with statistical errors. The analytic result of (5.3) is shown as a solid line while the lowest-order cross section is shown dotted.

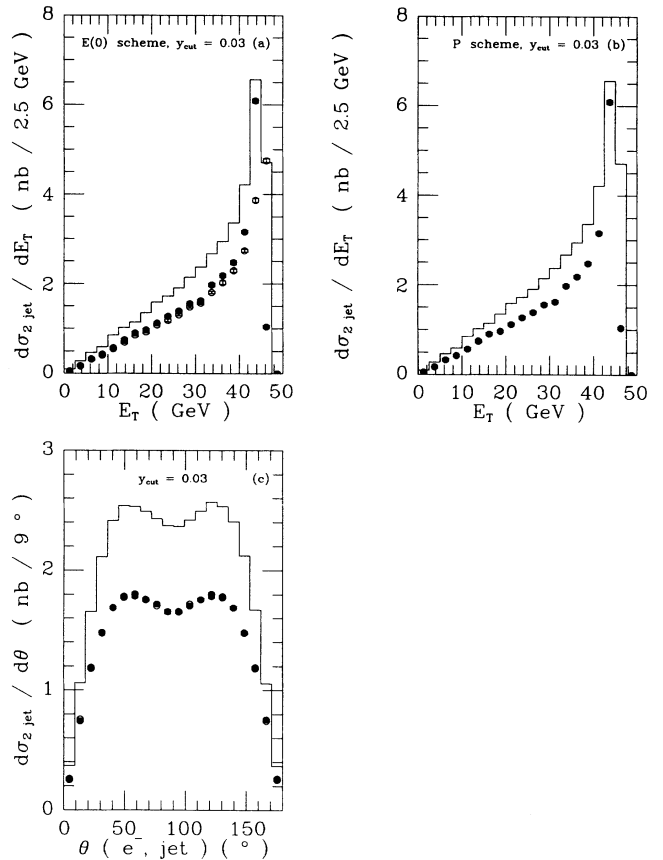


FIG. 2. The transverse-energy distribution at next-to-leading order in two-jet production for the hardest E_T jet (open points) and the softest E_T jet (solid points) for (a) the E/E_0 schemes and (b) the P scheme with statistical errors. At lowest order the hardest and softest E_T distributions coincide and are shown as a histogram. Part (c) shows the angular distribution of the jet with respect to the incoming electron at leading (histogram) and next-to-leading (points with statistical errors) order.

Figures 2(a) and 2(b) show the transverse energy distribution for the highest E_T jet (open points) and the lowest E_T jet (solid points). Although the two jets balance in E_T at leading order, this is not always the case at next-to-leading order. For example, in the E and $E0$ schemes [Fig. 2(a)] the transverse energies of the jets are not necessarily equal at next-to-leading order. This is a result of the fact that when a three-parton event is clustered to a two-jet event the energy of the “two parton” jet is equal to $|\mathbf{p}_1| + |\mathbf{p}_2|$, while the energy of the “one parton” jet has an energy equal to $|\mathbf{p}_1 + \mathbf{p}_2|$ which is smaller. On the other hand, in the P scheme [Fig. 2(b)] the “two-parton” jet energy is rescaled during the clustering (see Table I) such that its energy is equal to the softer “one-parton” jet. This also implies that the P scheme E_T distribution is equal to the soft E_T distribution in the E and $E0$ schemes.

Figure 2(c) shows the angular distribution between the jets and the incoming electron beam. We see that the shape of the angular distribution is unchanged by the next-to-leading-order corrections. Furthermore, there is no jet scheme dependence. This is readily understood by inspecting the jet algorithms of (5.2). Since the angular distribution depends only on the direction of the jet axis momentum vector it is unaffected by the momentum rescaling factor β and the two jet momentum vectors are always back to back.

B. Monte Carlo results for $e^+e^- \rightarrow 3$ jets

Just as in the two-jet Monte Carlo simulation discussed in the previous subsection, the next-to-leading order correction to three-jet production is built up of two contributions, the next-to-leading-order three-parton contributions and the leading-order four-parton contributions. Both of these processes can also contribute to the second-order two-jet cross section. This makes the next-to-leading-order three-jet cross section sensitive to the details of the jet algorithm, since the four-parton \rightarrow two-jet transition involves a double clustering, and is therefore sensitive to the cluster recombination scheme used (see Table I).

First of all we have to determine the right y_{\min}/y_{cut} ratio such that we are in the statistically dominated region and we show the y_{\min} dependence of the next-to-leading order three-jet cross section in Figs. 3(a), 3(b), and 3(c) for different y_{cut} values. The y_{\min} behavior is clearly much more complex than in the two-jet case of Fig. 1. This is readily understood from the three-parton resolved cross section of (4.26) where we see a complex interaction between the hard invariants and the cutoff y_{\min} . This is absent in the two-jet case (4.22) since there the only hard invariant mass, $s_{Q_1\bar{Q}_2}$, is equal to the center of mass energy. Nevertheless, we see that taking $y_{\min} = y_{\text{cut}}/100$ ensures that we are in the statistically dominated region while keeping the statistical error as small as possible with $10 \times (10000 + 100000)$ events.

In Fig. 3(d) we show how the statistical error depends on the specific value of y_{cut} for the three-jet cross section

at next-to-leading order using the E scheme (the dotted line indicates the leading-order three-jet cross section). As expected, the statistical error steadily grows with decreasing y_{cut} , due to the worsening cancellation of the y_{\min} dependence between the three- and four-parton cross sections.

One important motivation for calculating the next-to-leading-order corrections to the three-jet cross section is the expected reduction in the renormalization scale dependence. This scale dependence, indicated by μ , is shown in Fig. 4 for several values of y_{cut} . The dotted lines indicate the leading-order behavior, generically described by

$$d\sigma_{3\text{ jet}}^{\text{LO}} = \left(\frac{\alpha_s(\mu^2)}{2\pi} \right) dA. \quad (5.6)$$

The next-to-leading order corrections have the canonical form

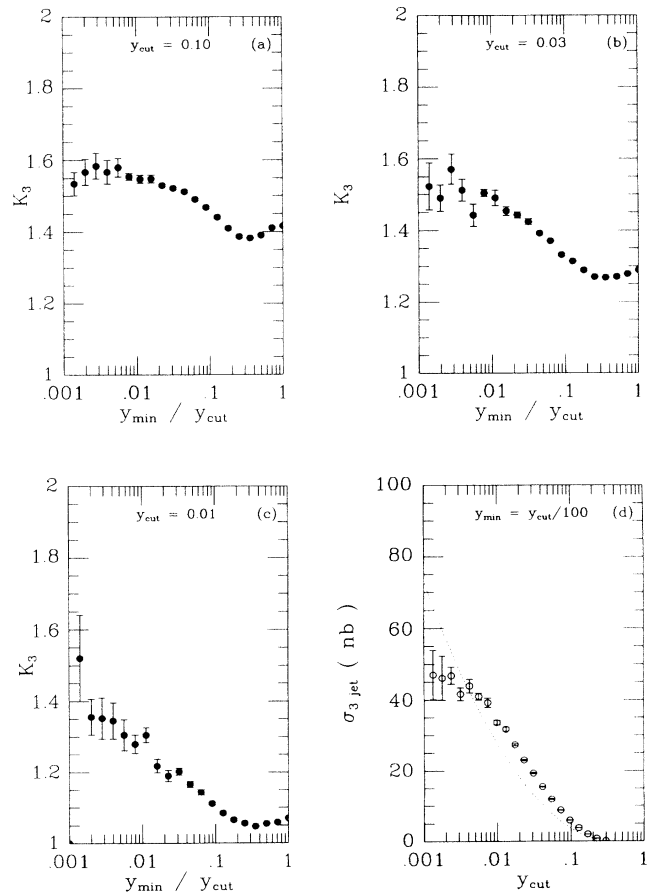


FIG. 3. The next-to-leading-order K factor, $K_3 = \sigma^{\text{NLO}}/\sigma^{\text{LO}}$, for three-jet production as a function of y_{\min}/y_{cut} for (a) $y_{\text{cut}} = 0.10$, (b) $y_{\text{cut}} = 0.03$ and (c) $y_{\text{cut}} = 0.01$ with statistical errors. Part (d) shows the y_{cut} dependence of the next-to-leading-order three-jet cross section in the E scheme for $y_{\min}/y_{\text{cut}} = 0.01$ with statistical errors. The leading-order three-jet cross section is shown as a dotted line.

$$d\sigma_{3 \text{ jet}}^{\text{NLO}} = \left(\frac{\alpha_s(\mu^2)}{2\pi} \right) \left\{ \left[1 + \alpha_s(\mu^2) b_0 \ln \left(\frac{\mu^2}{s_{\text{min}}} \right) \right] dA + \left(\frac{\alpha_s(\mu^2)}{2\pi} \right) dB \right\}. \quad (5.7)$$

The logarithmic term proportional to the leading-order result is generated by coupling constant renormalization and is the term which reduces the scale dependence of the coupling constant, thus rendering the next-to-leading-order three-jet cross section less dependent on the renormalization scale. It is worth noting that only the term proportional to the leading-order part dA has a reduced scale sensitivity. The term dB , which contains the finite virtual corrections to the three-parton cross section and the four-parton contributions, has, at this order, no reduction in scale dependence. This explains the rather different scale dependence at next-to-leading order for different choices of y_{cut} . For very small $y_{\text{cut}} = 0.004$ [Fig. 4(d)] the reduction is most significant, since the four-parton content in the three-jet cross section is strongly reduced. Increasing y_{cut} will increase the four-parton contribution, thereby increasing the scale sensitivity. This is clearly shown in Figs. 4(a)–4(c). Note that even in Fig. 4(a), with $y_{\text{cut}} = 0.10$ there is still a reduction in scale dependence.

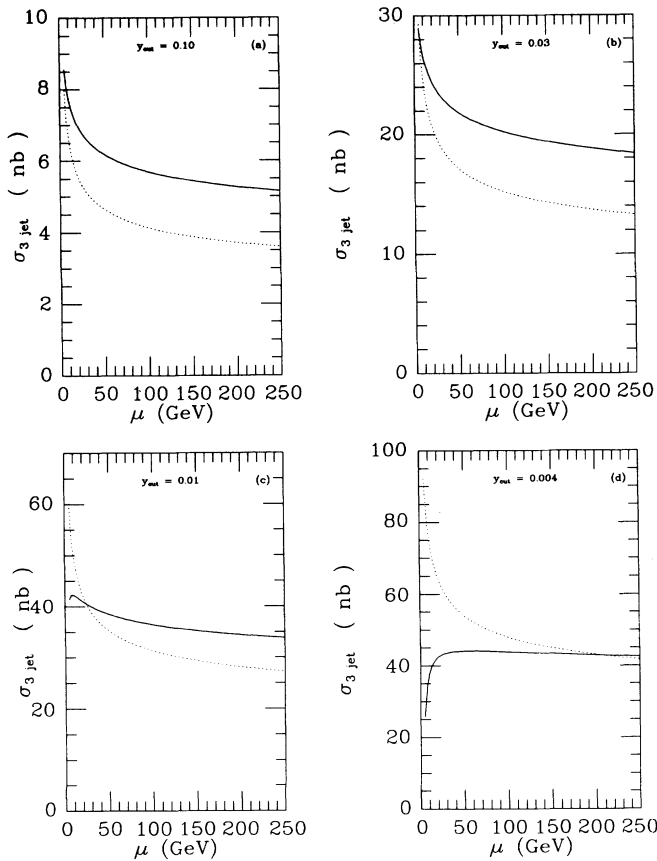


FIG. 4. The renormalization scale (μ) dependence of the leading-order (dotted line) and next-to-leading-order (solid line) three-jet cross section in the E scheme for (a) $y_{\text{cut}} = 0.10$, (b) $y_{\text{cut}} = 0.03$, (c) $y_{\text{cut}} = 0.01$, and (d) $y_{\text{cut}} = 0.004$.

Direct comparison of the Monte Carlo data with the experimental data is difficult without exact knowledge of the experimental situation. However it is of interest to see how well the experimental hadronic data, corrected for detector acceptance, compares with next-to-leading-order parton level calculations. One particularly interesting quantity is the jet fraction for which it is quite straightforward to make this comparison and see how well fixed order perturbative calculations compare with real hadronic data.

The n -jet fraction $f_n(y_{\text{cut}})$ is defined by

$$f_n(y_{\text{cut}}) = \frac{\sigma_{n \text{ jet}}(y_{\text{cut}})}{\sum_m \sigma_{m \text{ jet}}(y_{\text{cut}})} = \frac{\sigma_{n \text{ jet}}(y_{\text{cut}})}{\sigma_{\text{had}}}. \quad (5.8)$$

With the trivial identity $\sum_m f_m(y_{\text{cut}}) = 1$ we can use the calculated three- and four-jet cross sections [both at $O(\alpha_s^2)$] and total hadronic cross section σ_{had} at $O(\alpha_s^2)$ [41] to calculate the two jet fraction $f_2(y_{\text{cut}})$ at the same order. Fig. 5 shows prediction for the three [$O(\alpha_s^2)$] jet

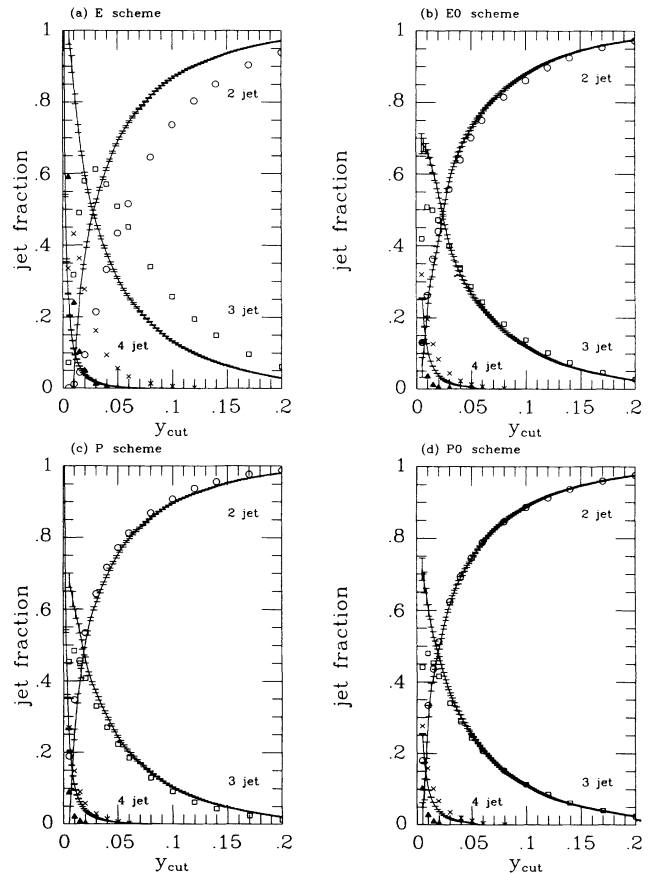


FIG. 5. Comparison of the $O(\alpha_s^2)$ parton level two-, three-, and four-jet fractions (solid lines with statistical error bars) with the hadronic data (points) as given by the OPAL Collaboration [3] in the (a) E scheme, (b) $E0$ scheme, (c) P scheme and the (d) $P0$ scheme.

fractions for several schemes [42] as solid lines (with error band) together with the hadronic jet fractions as tabulated by the OPAL Collaboration in Ref. [3] (points). As before, we choose $y_{\min} = y_{\text{cut}}/100$ and generate $10 \times (10\,000 + 100\,000)$ events.

From Fig. 5 we immediately see that not all jet algorithms work equally well for comparing the hadronic data with the fixed order calculation. In particular, the E scheme [Fig. 5(a)] does very poorly. Note that this is the only scheme which does not retain the masslessness of the recombined vector during the clustering phase. The other three schemes do as well as can be expected from an order- α_s^2 comparison with the data. The $E0$ scheme [Fig. 5(b)] underestimates the three-jet fraction somewhat, while the P scheme overestimates the three-jet fraction by a similar amount. The $P0$ scheme agrees remarkably well with the data. Whether deviations between the data and the calculation are due to hadronization effects or higher-order effects is impossible to tell from the calculation.

We notice that for $y_{\text{cut}} \lesssim 0.02$, the QCD calculation does not reproduce the data. This is not a surprise since we expect a deviation from the experimental data for small y_{cut} in perturbative calculations. This is, in a sense, associated with the growing five-jet contribution, which is not included in a theoretical $O(\alpha_s^2)$ calculation. More precisely, for small y_{cut} , terms $O(\alpha_s^2 \ln^{2n-1}(y_{\text{cut}}))$ are no longer small and have to be resummed [43].

Finally, in Fig. 6, we show all relevant angular correlations of the three-jet system in the P scheme. The jets are ordered according to their energies, jet 1 being the most energetic jet and jet 3 the least energetic. As

before, we generate $10 \times (10\,000 + 100\,000)$ events with $y_{\min} = y_{\text{cut}}/100$. The leading-order result is shown as a solid histogram, while the next-to-leading-order results are shown as points together with the estimate of the statistical error.

Figures 6(a)–6(c) show the angular differential cross sections amongst the three jets. Compared to leading order, there are slight deviations in the shape at next-to-leading order. For instance in Fig. 6(c) we see that the distribution obtains tails, which were “forbidden” at leading order due to energy-momentum conservation. Similar changes are present in Figs. 6(a) and 6(b).

The angles of the three jets with respect to the incoming electron beam are shown in Figs. 6(d)–6(f). The two most energetic jets [Figs. 6(d) and 6(e)] retain a characteristic “two-jet” shape [compare with Fig. 2(c)]. This is understood by realizing that these jets are predominantly formed from quarks, while the gluonic jet is usually the softest jet. These effects seem to be maintained at next-to-leading order, where the identification of a jet with a particular parton is no longer clear.

VI. CONCLUSIONS AND OUTLOOK

The main motivation for this paper has been to set up an explicit and general method of dealing with the final-state infrared and collinear divergences contributing to the next-to-leading-order corrections to multijet events, while avoiding algebraic and combinatorial complexities. Furthermore the method allows a numerical evaluation of phase space, making it possible to implement jet algorithms, detector acceptance, etc., numerically resulting

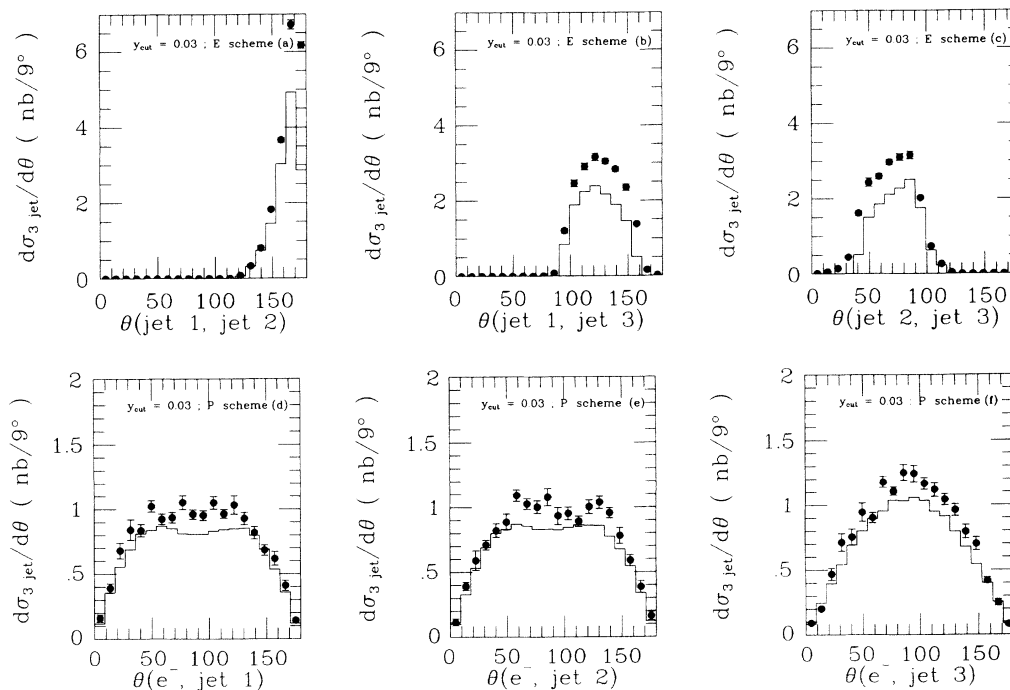


FIG. 6. The next-to-leading-order jet-jet and jet- e^- angular distributions in three-jet events with statistical errors. Jet 1 is the most energetic jet and jet 3 the softest jet. The jet-jet distributions are shown in the E scheme with $y_{\text{cut}} = 0.03$ and $y_{\min}/y_{\text{cut}} = 0.01$, while the jet- e^- distributions are shown in the P scheme. The leading-order result is shown as a histogram.

in very flexible Monte Carlo programs, as was explicitly shown in Sec. V.

The divergent soft and collinear factors are independent of the hard process, which means they can be applied to any scattering process involving final-state partons. Because of the factorization of the singular contributions of the matrix elements one obtains a cancellation of the soft and collinear divergences against the virtual divergences without specifying the hard process. In fact, it is straightforward to extract the soft singularities from the virtual graphs, as was shown in Sec. IV. Because of the factorization we can avoid squaring the resolved matrix elements in d dimensions altogether, which is a valuable simplification of the calculation. We can simply evaluate the resolved matrix elements using the standard methods developed for tree level matrix elements, such as helicity methods [18], recursivity [20, 10], etc. Furthermore, because of the factorization, the structure of the next-to-leading-order corrections in QCD is now transparent and systematic.

With the method described in this paper only the virtual graphs remain to be calculated, although a lot of the singular behavior of these graphs can be understood. We have explicitly recalculated the one-loop helicity amplitudes for $e^+e^- \rightarrow 2$ and 3 partons [44]. It was then straightforward to construct the Monte Carlo programs for the fully differential $e^+e^- \rightarrow 2$ and 3 jet cross sections. We found it unnecessary to write a sophisticated phase space generator, a simple importance sampling over the final-state invariants being sufficient, although this procedure might need to be improved upon if we want to include more final-state jets at the next-to-leading order.

The next obvious step is to include initial state partons, which necessitates a careful treatment of the initial-state collinear divergences in relation to the parton structure functions while keeping the hard process fully differential. Once this is understood, we can extend the method to processes involving multijet final states in deep inelastic and proton-antiproton collisions. For example, the processes

$$p\bar{p} \rightarrow W/Z + 0, 1 \text{ jets} \rightarrow \ell\bar{\ell} + 0, 1 \text{ jets}, \quad (6.1)$$

and

$$ep \rightarrow \ell + 1, 2 \text{ jets}, \quad (6.2)$$

at next-to-leading order are obtained by crossing the resolved matrix elements given in Sec. V.

ACKNOWLEDGMENTS

We are pleased to acknowledge useful discussions with F. A. Berends, R. K. Ellis, D. Kosower, T. Matsuura, and W. L. van Neerven. We are also happy to acknowledge financial support from the Texas National Research Laboratory Commission.

APPENDIX A: MATRIX ELEMENTS RELEVANT FOR $E^+E^- \rightarrow 2$ AND 3 JETS

In this appendix we provide a representation of the matrix elements for $e^+e^- \rightarrow 2, 3,$ and 4 partons which are relevant for $e^+e^- \rightarrow 2$ and 3 jet production at next-to-leading order. Since all poles in ϵ have been canceled we may evaluate these currents in 4 dimensions. A convenient method to evaluate matrix elements is using a helicity basis based on Weyl-van der Waerden spinors which is described in detail in [45, 7].

1. Weyl-van der Waerden spinor calculus

The basic quantity is the two-spinor ψ_A or ψ^A and its complex conjugate $\psi_{\dot{A}}$ or $\psi^{\dot{A}}$. Raising and lowering of indices is done with the antisymmetric tensor ϵ :

$$\epsilon_{AB} = \epsilon^{AB} = \epsilon_{\dot{A}\dot{B}} = \epsilon^{\dot{A}\dot{B}} = \begin{pmatrix} 0 & 1 \\ -1 & 0 \end{pmatrix}. \quad (A1)$$

We define an antisymmetric spinorial ‘‘inner product,’’

$$\langle \psi_1 \psi_2 \rangle = \psi_{1A} \epsilon^{BA} \psi_{2B} = \psi_{1A} \psi_2^A = -\psi_1^A \psi_{2A} = -\langle \psi_2 \psi_1 \rangle, \quad (A2)$$

and

$$\langle \psi_1 \psi_2 \rangle^* = \psi_{1\dot{A}} \psi_2^{\dot{A}}. \quad (A3)$$

Any momentum vector K_μ gets a bispinor representation by contraction with σ^μ :

$$K_{\dot{A}B} = \sigma_{\dot{A}B}^\mu K_\mu = \begin{pmatrix} K_0 + K_3 & K_1 + iK_2 \\ K_1 - iK_2 & K_0 - K_3 \end{pmatrix}, \quad (A4)$$

where σ^0 is the unit matrix and σ_i are the Pauli matrices. Since

$$\sigma_{\dot{A}B}^\mu \sigma^{\nu\dot{A}B} = 2g^{\mu\nu}, \quad (A5)$$

we have

$$K_{\dot{A}B} P^{\dot{A}B} = 2K \cdot P. \quad (A6)$$

For lightlike vectors one can show that

$$K_{\dot{A}B} = k_{\dot{A}} k_B, \quad (A7)$$

where

$$k_A = \left(\frac{(K_1 - iK_2)/\sqrt{K_0 - K_3}}{\sqrt{K_0 - K_3}} \right), \quad (A8)$$

such that for lightlike vectors (A6) becomes

$$2K \cdot P = \langle kp \rangle \langle kp \rangle^* = |\langle kp \rangle|^2. \quad (A9)$$

We usually denote four-momenta by upper case and the related spinors by lower case letters.

For massless spin- $\frac{1}{2}$ particles the four-spinors can be expressed in two-spinors as

$$\begin{aligned}
u_+(P) &= v_-(P) = \begin{pmatrix} p_B \\ 0 \end{pmatrix}, \\
u_-(P) &= v_+(P) = \begin{pmatrix} 0 \\ p_B \end{pmatrix}, \\
\bar{u}_+(Q) &= \bar{v}_-(Q) = (0, -iq_A), \\
\bar{u}_-(Q) &= \bar{v}_+(Q) = (iq^A, 0).
\end{aligned} \tag{A10}$$

The γ matrices now become

$$\gamma^\mu = \begin{pmatrix} 0 & -i\sigma_{BA}^\mu \\ i\sigma^{\mu AB} & 0 \end{pmatrix}, \tag{A11}$$

so that, e.g.,

$$\bar{u}_+(Q)\gamma^\mu v_-(P) = q_A \sigma^{\mu AB} p_B. \tag{A12}$$

The general electroweak vertex for vector boson V coupling to two fermions is denoted by $ie\delta_{ij}\Gamma_\mu^{Vf_1f_2}$, where i and j are the color labels associated with the fermions f_1 and f_2 respectively. The vertex contains left- and right-handed couplings:

$$\Gamma_\mu^{V,f_1f_2} = L_{f_1f_2}^V \gamma_\mu \left(\frac{1-\gamma_5}{2} \right) + R_{f_1f_2}^V \gamma_\mu \left(\frac{1+\gamma_5}{2} \right), \tag{A13}$$

where, for a photon,

$$L_{f_1f_2}^\gamma = R_{f_1f_2}^\gamma = -Q_{f_1} \delta_{f_1f_2}, \tag{A14}$$

and, for a Z boson,

$$\begin{aligned}
L_{f_1f_2}^Z &= \frac{I_3^{f_1} - \sin^2\theta_W Q_{f_1}}{\sin\theta_W \cos\theta_W} \delta_{f_1f_2}, \\
R_{f_1f_2}^Z &= \frac{-\sin\theta_W Q_{f_1}}{\cos\theta_W} \delta_{f_1f_2}.
\end{aligned} \tag{A15}$$

Here, Q_f represents the fractional electric charge, I_3^f the weak isospin, and θ_W the weak mixing angle. In the Weyl-van der Waerden notation, the vertex Γ_μ^{V,f_1f_2} becomes

$$\Gamma_\mu^{V,f_1f_2} = \begin{pmatrix} 0 & -iL_{f_1f_2}^V \sigma_{\mu\dot{B}A} \\ iR_{f_1f_2}^V \sigma_\mu^{\dot{A}B} & 0 \end{pmatrix}. \tag{A16}$$

For the polarization vectors of outgoing gluons and photons we use the spinorial quantities

$$e_{AB}^+(K) = \sqrt{2} \frac{k_A b_B}{\langle bk \rangle}, \tag{A17}$$

$$e_{AB}^-(K) = \sqrt{2} \frac{b_A k_B}{\langle bk \rangle^*}. \tag{A18}$$

The gauge spinor b is arbitrary and can be chosen differently in each gauge invariant expression. A suitable choice can often simplify the calculation.

The following relation is often useful:

$$\sigma_{AB}^\mu \sigma_{\dot{C}D}^\mu = 2\delta_A^{\dot{C}} \delta_B^D. \tag{A19}$$

2. Tree-level matrix elements for $e^+e^- \rightarrow 2, 3,$ and 4 partons

At lowest order, and including all orders in the number of colors, the squared matrix elements for $e^+e^- \rightarrow q\bar{q}+ng$ for $n = 0, 1,$ and 2 are given by

$$|\widehat{S}_\mu(Q_1; \bar{Q}_2)V^\mu|^2 = e^2 N |\mathcal{S}_\mu(Q_1; \bar{Q}_2)V^\mu|^2, \tag{A20}$$

$$|\widehat{S}_\mu(Q_1; 1; \bar{Q}_2)V^\mu|^2 = e^2 \left(\frac{g^2 N}{2} \right) \left(\frac{N^2 - 1}{N} \right) |\mathcal{S}_\mu(Q_1; 1; \bar{Q}_2)V^\mu|^2, \tag{A21}$$

and

$$|\widehat{S}_\mu(Q_1; 1, 2; \bar{Q}_2)V^\mu|^2 = e^2 \left(\frac{g^2 N}{2} \right)^2 \left(\frac{N^2 - 1}{N} \right) \left[\sum_{P(1,2)} |\mathcal{S}_\mu(Q_1; 1, 2; \bar{Q}_2)V^\mu|^2 - \frac{1}{N^2} |\mathcal{S}_\mu(Q_1; \bar{1}, \bar{2}; \bar{Q}_2)V^\mu|^2 \right], \tag{A22}$$

respectively. In the two-quark two-gluon process (A22),

$$\mathcal{S}_\mu(Q_1; \bar{1}, \bar{2}; \bar{Q}_2) = \mathcal{S}_\mu(Q_1; 1, 2; \bar{Q}_2) + \mathcal{S}_\mu(Q_1; 2, 1; \bar{Q}_2). \tag{A23}$$

We can use the spinor calculus of the previous section to express the lepton current V_μ in terms of the helicities of the incident e^+ and e^- (with momenta P^+ and P^- respectively). Explicitly,

$$V_\mu^\gamma(e^+, e^-) = e\sigma_\mu^{\dot{A}B} p_A^- p_B^+ \frac{L_{ee}^\gamma}{s}, \quad V_\mu^Z(e^+, e^-) = e\sigma_\mu^{\dot{A}B} p_A^- p_B^+ \frac{L_{ee}^Z}{s - M_Z^2 + i\Gamma_Z M_Z}, \tag{A24}$$

$$V_\mu^\gamma(e^+, e^-) = e\sigma_\mu^{\dot{A}B} p_A^+ p_B^- \frac{R_{ee}^\gamma}{s}, \quad V_\mu^Z(e^+, e^-) = e\sigma_\mu^{\dot{A}B} p_A^+ p_B^- \frac{R_{ee}^Z}{s - M_Z^2 + i\Gamma_Z M_Z}.$$

Note that the full matrix element for any process is summed over both photon and Z -boson exchange.

The hadronic current S_μ is given by

$$S_\mu(Q_1+; 1\lambda_1, \dots, n\lambda_n; \bar{Q}_2-) = R_{f_1 f_2}^V (\sqrt{2})^n \sigma_\mu^{AB} S_{AB}(Q_1+; 1\lambda_1, \dots, n\lambda_n; \bar{Q}_2-), \quad (\text{A25})$$

$$S_\mu(Q_1-; 1\lambda_1, \dots, n\lambda_n; \bar{Q}_2+) = L_{f_1 f_2}^V (\sqrt{2})^n \sigma_\mu^{AB} S_{AB}(Q_1-; 1\lambda_1, \dots, n\lambda_n; \bar{Q}_2+). \quad (\text{A26})$$

We list here the quantities $S_{AB}(Q_1+; 1\lambda_1, \dots, n\lambda_n; \bar{Q}_2-)$ for $n = 0, 1$, and 2. The currents with the quark helicities flipped follows from parity conservation:

$$S_{AB}(Q_1-; 1\lambda_1, \dots, n\lambda_n; \bar{Q}_2+) = (S_{BA}(Q_1+; 1(-\lambda_1), \dots, n(-\lambda_n); \bar{Q}_2-))^*. \quad (\text{A27})$$

Charge conjugation implies the following relations between currents with different helicities:

$$S_{AB}(Q_1\lambda_{Q_1}; 1\lambda_1, \dots, n\lambda_n; \bar{Q}_2\lambda_{\bar{Q}_2}) = (-1)^n S_{AB}(\bar{Q}_2\lambda_{\bar{Q}_2}; n\lambda_n, \dots, 1\lambda_1; Q_1\lambda_{Q_1}). \quad (\text{A28})$$

The following notation will also be useful:

$$\langle a|B+C|d\rangle = a_{\dot{E}} d_F (B+C)^{\dot{E}F} = \langle ab\rangle^* \langle db\rangle + \langle ac\rangle^* \langle dc\rangle, \quad (\text{A29})$$

where the last step only holds for lightlike vectors. All helicity amplitudes are related to the amplitudes with $\lambda_{Q_1} = +$ and $\lambda_{\bar{Q}_2} = -$. First of all, at tree level, we have the trivial $n = 0$ result

$$S_{AB}(Q_1+; \bar{Q}_2-) = q_{1A} \bar{q}_{2B}. \quad (\text{A30})$$

Secondly, the $n = 1$ result is

$$S_{AB}(Q_1+; 1+; \bar{Q}_2-) = \frac{(Q_1 + K_1)_{AD} \bar{q}_2^D \bar{q}_{2B}}{\langle q_1 k_1 \rangle \langle k_1 \bar{q}_2 \rangle}. \quad (\text{A31})$$

Thirdly, for $n = 2$ we have three helicity combinations

$$\begin{aligned} S_{AB}(Q_1+; 1+2+; \bar{Q}_2-) &= \frac{(Q_1 + K_1 + K_2)_{AD} \bar{q}_2^D \bar{q}_{2B}}{\langle q_1 k_1 \rangle \langle k_1 k_2 \rangle \langle k_2 \bar{q}_2 \rangle}, \\ S_{AB}(Q_1+; 1+2-; \bar{Q}_2-) &= -\frac{\langle q_1 k_1 \rangle^* \langle q_1 k_2 \rangle (Q_1 + K_1)_{AD} k_2^D \bar{q}_{2B}}{\langle q_1 k_1 \rangle (K_1 + K_2)^2 (Q_1 + K_1 + K_2)^2} + \frac{\langle k_1 \bar{q}_2 \rangle^* \langle k_2 \bar{q}_2 \rangle q_{1A} (K_2 + \bar{Q}_2)_{CB} k_1^C}{\langle k_2 \bar{q}_2 \rangle^* (K_1 + K_2)^2 (K_1 + K_2 + \bar{Q}_2)^2} \\ &\quad - \frac{(Q_1 + K_1)_{AD} k_2^D (K_2 + \bar{Q}_2)_{CB} k_1^C}{\langle q_1 k_1 \rangle \langle k_2 \bar{q}_2 \rangle^* (K_1 + K_2)^2}, \\ S_{AB}(Q_1+; 1-2+; \bar{Q}_2-) &= \frac{\langle k_1 \bar{q}_2 \rangle^2 q_{1A} (K_1 + \bar{Q}_2)_{CB} k_2^C}{\langle k_2 \bar{q}_2 \rangle (K_1 + K_2)^2 (K_1 + K_2 + \bar{Q}_2)^2} - \frac{\langle q_1 k_2 \rangle^* (Q_1 + K_2)_{AD} k_1^D \bar{q}_{2B}}{\langle q_1 k_1 \rangle^* (K_1 + K_2)^2 (Q_1 + K_1 + K_2)^2} \\ &\quad + \frac{\langle k_1 \bar{q}_2 \rangle \langle q_1 k_2 \rangle^* q_{1A} \bar{q}_{2B}}{\langle q_1 k_1 \rangle^* \langle k_2 \bar{q}_2 \rangle (K_1 + K_2)^2}. \end{aligned} \quad (\text{A32})$$

Finally, the lowest-order matrix elements for $e^+ e^- \rightarrow q \bar{q} q \bar{q}$ at all orders in the number of colors are given by

$$\begin{aligned} \left| \widehat{T}_\mu(Q_1, \bar{Q}_2; Q_3, \bar{Q}_4) V^\mu \right|^2 &= e^2 \left(\frac{g^2 N}{2} \right)^2 \left(\frac{N^2 - 1}{N^2} \right) \\ &\quad \times \left[\left| \mathcal{X}_\mu(Q_1, \bar{Q}_2; Q_3, \bar{Q}_4) V^\mu \right|^2 + \left| \mathcal{X}_\mu(Q_1, \bar{Q}_4; Q_3, \bar{Q}_2) V^\mu \right|^2 \right. \\ &\quad \left. + \frac{2}{N} \text{Re} \left\{ \mathcal{X}_\mu(Q_1, \bar{Q}_2; Q_3, \bar{Q}_4) V^\mu (\mathcal{X}_\nu(Q_1, \bar{Q}_4; Q_3, \bar{Q}_2) V^\nu)^\dagger \right\} \right], \end{aligned} \quad (\text{A33})$$

where

$$\mathcal{X}_\mu(Q_1, \bar{Q}_2; Q_3, \bar{Q}_4) = A_\mu(Q_1, \bar{Q}_4; Q_3, \bar{Q}_2) + A_\mu(Q_3, \bar{Q}_2; Q_1, \bar{Q}_4). \quad (\text{A34})$$

The leptonic current is given by (A24) while A_μ is given by

$$A_\mu(Q_1 + \bar{Q}_4 \lambda_{Q_4}; Q_3 \lambda_{Q_3} \bar{Q}_2-) = R_{f_1 f_2}^V \sigma_\mu^{AB} A_{AB}(Q_1 + \bar{Q}_4 \lambda_{Q_4}; Q_3 \lambda_{Q_3} \bar{Q}_2-), \quad (\text{A35})$$

$$A_\mu(Q_1 - \bar{Q}_4 \lambda_{Q_4}; Q_3 \lambda_{Q_3} \bar{Q}_2+) = L_{f_1 f_2}^V \sigma_\mu^{AB} A_{AB}(Q_1 - \bar{Q}_4 \lambda_{Q_4}; Q_3 \lambda_{Q_3} \bar{Q}_2+).$$

As in the two-quark case, the helicity amplitudes with flipped helicities are obtained from the parity relation

$$A_{\dot{A}B}(Q_1 - \lambda_{Q_1}\bar{Q}_4 - \lambda_{Q_4}; Q_3 - \lambda_{Q_3}\bar{Q}_2 - \lambda_{Q_2}) = (A_{\dot{B}A}(Q_1\lambda_{Q_1}\bar{Q}_4\lambda_{Q_4}; Q_3\lambda_{Q_3}\bar{Q}_2\lambda_{Q_2}))^*, \quad (\text{A36})$$

while charge conjugation yields the relations

$$\begin{aligned} A_{\dot{A}B}(Q_1\lambda_{Q_1}\bar{Q}_4\lambda_{Q_4}; Q_3\lambda_{Q_3}\bar{Q}_2\lambda_{Q_2}) &= A_{\dot{A}B}(\bar{Q}_2\lambda_{Q_2}\bar{Q}_4\lambda_{Q_4}; Q_3\lambda_{Q_3}Q_1\lambda_{Q_1}) \\ &= A_{\dot{A}B}(Q_1\lambda_{Q_1}, Q_3\lambda_{Q_3}; \bar{Q}_4\lambda_{Q_4}\bar{Q}_2\lambda_{Q_2}) \\ &= A_{\dot{A}B}(\bar{Q}_2\lambda_{Q_2}Q_3\lambda_{Q_3}; \bar{Q}_4\lambda_{Q_4}Q_1\lambda_{Q_1}). \end{aligned} \quad (\text{A37})$$

All helicity amplitudes are therefore determined by

$$A_{\dot{A}B}(Q_1 + \bar{Q}_4^-; Q_3 + \bar{Q}_2^-) = -\frac{\langle q_1 q_3 \rangle^* (Q_1 + Q_3)_{\dot{A}D} \bar{q}_4^D \bar{q}_{2B}}{(Q_3 + \bar{Q}_4)^2 (Q_1 + Q_3 + \bar{Q}_4)^2} + \frac{\langle \bar{q}_2 \bar{q}_4 \rangle q_{1\dot{A}} (\bar{Q}_2 + \bar{Q}_4)_{\dot{C}B} \dot{q}_3^{\dot{C}}}{(Q_3 + \bar{Q}_4)^2 (\bar{Q}_2 + Q_3 + \bar{Q}_4)^2}. \quad (\text{A38})$$

3. Next-to-leading-order matrix elements for $e^+e^- \rightarrow 2$ and 3 partons

As described in Sec. IV, the next-to-leading-order matrix elements for $e^+e^- \rightarrow q\bar{q}$ have the form

$$\left| \hat{\mathcal{S}}_\mu(Q_1; \bar{Q}_2) V^\mu \right|_F^2 = e^2 N \left(1 - \frac{1}{N^2} \right) \left[\mathcal{K}(Q_1; \bar{Q}_2) \left| S_\mu(Q_1; \bar{Q}_2) V^\mu \right|^2 + \mathcal{F}(Q_1; \bar{Q}_2) \right], \quad (\text{A39})$$

where, because of our assignment of the finite pieces [46],

$$\mathcal{F}(Q_1; \bar{Q}_2) = 0. \quad (\text{A40})$$

Helicity amplitudes for V_μ and $S_\mu(Q_1; \bar{Q}_2)$ are given in the previous section. The dynamical \mathcal{K} factor $\mathcal{K}(Q_1; \bar{Q}_2)$ is given by (4.22).

Similarly, the next-to-leading-order matrix elements for $e^+e^- \rightarrow q\bar{q} + g$ are given by

$$\left| \hat{\mathcal{S}}_\mu(Q_1; 1; \bar{Q}_2) V^\mu \right|_F^2 = e^2 \left(\frac{g^2 N}{2} \right) \left(\frac{N^2 - 1}{N} \right) \left[\left(\mathcal{K}(Q_1; 1; \bar{Q}_2) - \frac{1}{N^2} \mathcal{K}(Q_1; \bar{Q}_2) \right) \left| S_\mu(Q_1; 1; \bar{Q}_2) V^\mu \right|^2 + \mathcal{F}(Q_1; 1; \bar{Q}_2) \right], \quad (\text{A41})$$

where $\mathcal{K}(Q_1; 1; \bar{Q}_2)$ is given by (4.31) with $n = 1$. With this assignment of the finite contributions, we find

$$\mathcal{F}(Q_1; 1; \bar{Q}_2) = 2 \left(\frac{g^2 N}{2} \right) \text{Re} \left\{ (S_\mu(Q_1; 1; \bar{Q}_2) V^\mu) (\bar{S}_\nu^{(1)}(Q_1; 1; \bar{Q}_2) V^\nu)^\dagger \right\}. \quad (\text{A42})$$

The finite next-to-leading-order current $\bar{S}_\mu^{(1)}$ satisfies (A25)–(A28) [47]. Explicitly, we find

$$\begin{aligned} \left(\frac{g^2 N}{2} \right) \bar{S}_{\dot{A}B}^{(1)}(Q_{1+}; 1+; \bar{Q}_{2-}) &= \frac{\alpha_s(\mu^2) N}{4\pi} \left[\left(\alpha_0 - \frac{\alpha_2}{N^2} \right) \frac{Q_{1\dot{A}D} \bar{q}_2^D \bar{q}_{2B}}{\langle q_1 k_1 \rangle \langle k_1 \bar{q}_2 \rangle} + \left(\beta_0 - \frac{\beta_2}{N^2} \right) \frac{K_{1\dot{A}D} \bar{q}_2^D \bar{q}_{2B}}{\langle q_1 k_1 \rangle \langle k_1 \bar{q}_2 \rangle} \right. \\ &\quad \left. + \left(\gamma_0 - \frac{\gamma_2}{N^2} \right) \frac{Q_{1\dot{C}B} k_1^{\dot{C}} k_{1\dot{A}}}{\langle q_1 k_1 \rangle \langle k_1 \bar{q}_2 \rangle^*} \right]. \end{aligned} \quad (\text{A43})$$

The other helicity amplitudes are obtained from $\bar{S}_{\dot{A}B}^{(1)}(+; +; -)$ by the usual parity and charge conjugation relations, while the coefficients α_i , β_i , and γ_i are written in terms of the scaled invariant masses, $y_{ij} = s_{ij}/Q^2$:

$$\begin{aligned}
\alpha_0 &= -R(y_{Q_1 K_1}, y_{K_1 \bar{Q}_2}) - \frac{y_{K_1 \bar{Q}_2} (4 - 3y_{K_1 \bar{Q}_2})}{2(1 - y_{K_1 \bar{Q}_2})^2} \ln(y_{K_1 \bar{Q}_2}) - \frac{y_{K_1 \bar{Q}_2}}{2(1 - y_{K_1 \bar{Q}_2})} + \delta_0, \\
\beta_0 &= -R(y_{Q_1 K_1}, y_{K_1 \bar{Q}_2}) + \frac{4 - 3y_{K_1 \bar{Q}_2}}{2(1 - y_{K_1 \bar{Q}_2})} \ln(y_{K_1 \bar{Q}_2}) + 1 + \delta_0, \\
\gamma_0 &= +\frac{y_{K_1 \bar{Q}_2}}{2(1 - y_{K_1 \bar{Q}_2})^2} \ln(y_{K_1 \bar{Q}_2}) + \frac{y_{K_1 \bar{Q}_2}}{2(1 - y_{K_1 \bar{Q}_2})}, \\
\alpha_2 &= -R(y_{Q_1 \bar{Q}_2}, y_{Q_1 K_1}) - \frac{(1 - y_{Q_1 \bar{Q}_2})^2}{y_{Q_1 K_1}^2} R(y_{Q_1 \bar{Q}_2}, y_{K_1 \bar{Q}_2}) - \frac{y_{K_1 \bar{Q}_2}}{y_{Q_1 K_1}} \ln(y_{Q_1 \bar{Q}_2}) \\
&\quad - \left(\frac{y_{K_1 \bar{Q}_2} (4 - 3y_{K_1 \bar{Q}_2})}{2(1 - y_{K_1 \bar{Q}_2})^2} + \frac{y_{K_1 \bar{Q}_2}^2}{y_{Q_1 K_1} (1 - y_{K_1 \bar{Q}_2})} \right) \ln(y_{K_1 \bar{Q}_2}) - \frac{y_{K_1 \bar{Q}_2}}{2(1 - y_{K_1 \bar{Q}_2})} + \delta_2,
\end{aligned} \tag{A44}$$

$$\begin{aligned}
\beta_2 &= -R(y_{Q_1 \bar{Q}_2}, y_{Q_1 K_1}) + \left(\frac{y_{Q_1 \bar{Q}_2} (1 - y_{Q_1 \bar{Q}_2})}{y_{Q_1 K_1}^2} + \frac{1}{y_{Q_1 K_1}} \right) R(y_{Q_1 \bar{Q}_2}, y_{K_1 \bar{Q}_2}) \\
&\quad + \left(\frac{y_{Q_1 K_1}}{(1 - y_{Q_1 \bar{Q}_2})^2} + \frac{1 - y_{K_1 \bar{Q}_2}}{y_{Q_1 K_1}} \right) \ln(y_{Q_1 \bar{Q}_2}) + \left(\frac{4 - 3y_{K_1 \bar{Q}_2}}{2(1 - y_{K_1 \bar{Q}_2})} + \frac{y_{K_1 \bar{Q}_2}}{y_{Q_1 K_1}} \right) \ln(y_{K_1 \bar{Q}_2}) + \frac{y_{Q_1 K_1}}{(1 - y_{Q_1 \bar{Q}_2})} + \delta_2, \\
\gamma_2 &= +\frac{y_{K_1 \bar{Q}_2}}{y_{Q_1 K_1}^2} R(y_{Q_1 \bar{Q}_2}, y_{K_1 \bar{Q}_2}) - \left(\frac{y_{Q_1 K_1}}{(1 - y_{Q_1 \bar{Q}_2})^2} - \frac{1}{y_{Q_1 K_1}} \right) \ln(y_{Q_1 \bar{Q}_2}) \\
&\quad + \left(\frac{y_{K_1 \bar{Q}_2}}{2(1 - y_{K_1 \bar{Q}_2})^2} + \frac{y_{K_1 \bar{Q}_2}}{y_{Q_1 K_1} (1 - y_{K_1 \bar{Q}_2})} \right) \ln(y_{K_1 \bar{Q}_2}) + \frac{y_{K_1 \bar{Q}_2}}{(1 - y_{Q_1 \bar{Q}_2})} + \frac{y_{K_1 \bar{Q}_2}}{2(1 - y_{K_1 \bar{Q}_2})},
\end{aligned}$$

where the function $R(x, y)$ is defined in terms of the dilogarithm (5.5) as

$$R(x, y) = \ln(x) \ln(y) - \ln(x) \ln(1 - x) - \ln(y) \ln(1 - y) + \frac{\pi^2}{6} - \text{Li}_2(x) - \text{Li}_2(y). \tag{A45}$$

The coefficients δ_i are given by

$$\delta_0 = -\frac{3}{4} \ln(y_{Q_1 K_1}) - \frac{3}{4} \ln(y_{K_1 \bar{Q}_2}), \quad \delta_2 = -\frac{3}{2} \ln(y_{Q_1 \bar{Q}_2}), \tag{A46}$$

and are generated by our choice of V_{ij}^{col} (4.20). For example, the choice

$$V_{g\bar{q}}^{\text{col}} = V_{g\bar{q}}^{\text{col}} = \frac{1}{2} V_{g\bar{q}}^{\text{col}} = -\frac{3}{4\epsilon} - 2 \tag{A47}$$

corresponds to

$$\delta_0 = \delta_2 = 0, \tag{A48}$$

and with the appropriate changes in $\mathcal{K}(Q_1; \bar{Q}_2)$ and $\mathcal{K}(Q_1; 1; \bar{Q}_2)$ reproduces the results of [16] when multiplied by $\mathcal{S}_\mu(Q_1; 1; \bar{Q}_2)$.

-
- [1] UA2 Collaboration, presented by P. Lubrano, in *Proceedings of the 4th Rencontres de Physique de la Vallée d'Aoste*, La Thuile, Italy, 1990, edited by M. Greco (Editions Frontieres, Singapore, 1990), p. 355.
- [2] CDF Collaboration, presented by S. Geer, in *8th INFN Eloisatron Project Workshop on the Higgs Boson*, Erice, Italy, 1989, edited by A. Ali (Plenum, New York, 1990), p. 447.
- [3] DELPHI Collaboration, P. Aarnio *et al.*, Phys. Lett. B **247**, 167 (1990); L3 Collaboration, B. Adeva *et al.*, *ibid.* **248**, 464 (1990); OPAL Collaboration, M. Akrawy *et al.*, Z. Phys. C **49**, 375 (1991).
- [4] B.L. Combridge, J. Kripfganz, and J. Ranft, Phys. Lett. **70B**, 234 (1977); R. Cutler and D. Sivers, Phys. Rev. D **17**, 196 (1978).
- [5] T. Gottschalk and D. Sivers, Phys. Rev. D **21**, 102 (1980); Z. Kunszt and E. Pietarinen, Nucl. Phys. **B164**, 45 (1980); F.A. Berends, R. Kleiss, P. de Causmaecker, R. Gastmans, and T.T. Wu, Phys. Lett. **103B**, 124 (1981).
- [6] J.F. Gunion and Z. Kunszt, Phys. Lett. **159B**, 167 (1985); Phys. Lett. B **176**, 163 (1986); Z. Kunszt, Nucl. Phys. **B271**, 333 (1986); J.F. Gunion and J. Kalinowski, Phys. Rev. D **34**, 2119 (1986); S.J. Parke and T.R. Taylor, Nucl. Phys. **B269**, 410 (1986); Phys. Rev. D **35**, 313 (1987).

- [7] F.A. Berends and W.T. Giele, Nucl. Phys. **B294**, 700 (1987).
- [8] M. Mangano, S.J. Parke, and Z. Xu, Nucl. Phys. **B298**, 653 (1988); **B299**, 673 (1988).
- [9] F.A. Berends, W.T. Giele, and H. Kuijf, Nucl. Phys. **B333**, 120 (1990).
- [10] J.G.M. Kuijf, Ph.D. thesis, Leiden, 1991.
- [11] R.K. Ellis and R.J. Gonsalves, in *Proceedings of the Workshop on Super High Energy Physics*, Eugene, Oregon, 1985, edited by D.E. Soper (World Scientific, Singapore, 1986); p. 287; R. Kleiss and W.J. Stirling, Nucl. Phys. **B262**, 235 (1985).
- [12] K. Hagiwara and D. Zeppenfeld, Nucl. Phys. **B313**, 560 (1989).
- [13] F.A. Berends, W.T. Giele, and H. Kuijf, Nucl. Phys. **B321**, 39 (1989).
- [14] F.A. Berends, W.T. Giele, H. Kuijf, and B. Tausk, Nucl. Phys. **B357**, 32 (1991).
- [15] A. Ali, J.G. Körner, G. Kramer, Z. Kunszt, G. Schierholtz, E. Pietarinen, and J. Willrodt, Nucl. Phys. **B167**, 454 (1980); D. Dankaert, P. de Causmaecker, R. Gastmans, W. Troost, and T.T. Wu, Phys. Lett. **114B**, 203 (1982).
- [16] R.K. Ellis, D.A. Ross, and A.E. Terrano, Nucl. Phys. **B178**, 421 (1981).
- [17] N.K. Falck, D. Graudenz, and G. Kramer, Nucl. Phys. **B328**, 317 (1989).
- [18] P. de Causmaecker, R. Gastmans, W. Troost, and T.T. Wu, Phys. Lett. **105B**, 215 (1981); R. Kleiss, Nucl. Phys. **B241**, 61 (1984); R. Kleiss and W.J. Stirling, *ibid.* **B262**, 235 (1985); Z. Xu, D.H. Zhang, and L. Chang, *ibid.* **B291**, 392 (1987).
- [19] D. Zeppenfeld, Int. J. Mod. Phys. A **3**, 2175 (1988).
- [20] F.A. Berends and W.T. Giele, Nucl. Phys. **B306**, 759 (1988).
- [21] G. 't Hooft and M. Veltman, Nucl. Phys. **B44**, 189 (1972).
- [22] C.G. Bollini and J.J. Giambiagi, Phys. Lett. **40B**, 566 (1972); J.F. Ashmore, Nuovo Cimento Lett. **4**, 289 (1972).
- [23] J. Kubar-Andre and F.E. Paige, Phys. Rev. D **19**, 221 (1979).
- [24] Z. Kunszt and P. Nason, in *Z Physics at LEP 1*, Proceedings of the Workshop, Geneva, Switzerland, 1989, edited by G. Altarelli, R. Kleiss, and C. Verzegnassi (CERN Yellow Report No. 89-08, Geneva, 1989), Vol. 1, p. 373.
- [25] G. Kramer and B. Lampe, Z. Phys. C **34**, 497 (1987).
- [26] The next-to-leading-order two-jet cross section was first analytically computed by G. Sterman and S. Weinberg, Phys. Rev. Lett. **39**, 1436 (1977).
- [27] F. Bloch and A. Nordsieck, Phys. Rev. **52**, 54 (1937).
- [28] T. Kinoshita, J. Math. Phys. **3**, 650 (1962); T.D. Lee and M. Nauenberg, Phys. Rev. **133**, 1549 (1964).
- [29] G. Sterman, Phys. Rev. D **17**, 2773 (1978); **17**, 2789 (1978).
- [30] F.A. Berends, K.J.F. Gaemers, and R. Gastmans, Nucl. Phys. **B57**, 381 (1973); F.A. Berends, R. Kleiss, and S. Jadach, *ibid.* **B202**, 63 (1982); W.L. van Neerven and J.A.M. Vermaseren, *ibid.* **B238**, 73 (1984).
- [31] H. Baer, J. Ohnemus, and J.F. Owens, Phys. Rev. D **40**, 2844 (1989); Phys. Lett. B **234**, 127 (1990); Phys. Rev. D **42**, 61 (1990).
- [32] F.A. Berends and W.T. Giele, Nucl. Phys. **B313**, 595 (1989).
- [33] M. Mangano, Nucl. Phys. **B309**, 461 (1988).
- [34] D.R. Yennie, S.C. Frautschi, and H. Suura, Ann. Phys. (N.Y.) **13**, 379 (1961).
- [35] A. Bassetto, M. Ciafaloni, and P. Marchesini, Phys. Rep. **100**, 201 (1983); M. Mangano and S. Parke, in *Proceedings of the International Europhysics Conference on High Energy Physics*, Uppsala, Sweden, 1987, edited by O. Botner (European Physical Society, Petit-Lancy, Switzerland, 1987), p. 201.
- [36] P. Cvitanovic, P.G. Lauwers, and P.N. Scharbach, Nucl. Phys. **B186**, 165 (1981).
- [37] G. Altarelli and G. Parisi, Nucl. Phys. **B126**, 298 (1977).
- [38] G. Kramer, *Theory of Jets in Electron-Positron Annihilation* (Springer-Verlag, Berlin, 1984).
- [39] G. Passarino and M. Veltman, Nucl. Phys. **B160**, 151 (1979).
- [40] W.A. Bardeen, A.J. Buras, D.W. Duke, and T. Muta, Phys. Rev. D **18**, 3998 (1978).
- [41] K.G. Chetrykin, A.L. Kateev, and F.V. Tkachov, Phys. Lett. **85B**, 277 (1979); M. Dine and J. Sapirstein, Phys. Rev. Lett. **43**, 668 (1979); W. Celmaster and R.J. Gonsalves, Phys. Rev. Lett. **44**, 560 (1979); Phys. Rev. D **21**, 3112 (1979).
- [42] Figure 5(d) is the jet fraction in the P0 scheme, which is equivalent to the P scheme except that after each clustering the total visible energy is recalculated from the final-state momenta and all the invariant masses are scaled by the visible energy rather than Q^2 .
- [43] S. Catani, G. Turnock, B.R. Webber, and L. Trentadue, Cambridge Report No. CAVENDISH-HEP-90-16, 1990 (unpublished).
- [44] To go beyond this in e^+e^- involves the evaluation of one-loop five-point integrals.
- [45] H. Weyl, *Gruppentheorie und Quantenmechanik* (Leipzig, 1928); B.L. van der Waerden, Goettinger Nachrichten, 100 (1929).
- [46] Since no anomalies are present, we take γ_5 to be anti-commuting in all d dimensions.
- [47] We note that the helicity amplitudes for this process have been evaluated by J.G. Körner and P. Sieben, Nucl. Phys. **B363**, 65 (1991).